The Numerical Solution of Free Surface/Pressurized Flow in Pipes

Ian MacDonald

September 1992

Submitted to the

Department of Mathematics,

University of Reading,

in partial fulfillment of the requirements for the

Degree of Master of Science

Abstract

Flows in closed channels can change from free surface flow to pressurized flow and vice versa. Normally we require two different sets of equations to model these different regimes, however with the use of a thin slot in the channel soffit, we can model both using only the open channel equations. When this is done numerically, using Roe's scheme, serious oscillations are observed in the time history of the solution. In this work, possible causes of these oscillations are investigated, and attempts are made to remove them.

Acknowledgements

I would like to thank Dr.M.J.Baines, Dr.A.Priestly and Dr.P.K.Sweby of the Mathematics Department, University of Reading, for their help, support and advice during this work.

I would also like to acknowledge the financial support of the SERC.

Contents

Chapter 1

Introduction

In a closed channel (pipe, channel with soffit) there are often situations which involve a transition from free surface flow to pressurized flow, or vice versa. For example if we have a closed channel in a hydraulic plant, with initially free surface flow, then the start-up of machinery (pumps, turbines) may cause a steep wave which in turn may give rise to pressurized flow conditions. Flows with this kind of transition are particularly hard to model because these two different flow regimes require different sets of equations to model them. This requires us to explicitly track any interface between the two different regimes, and solve the appropriate equations for each section. We shall see that by putting a thin vertical slot in the channel soffit we can simulate pressurized flow with the same equations as we model free surface flow. Hence we can model both flow regimes with this one set of conservation laws, the open channel equations. When we do this we no longer need keep track of any interfaces between flow regimes, since all sections of the flow are modelled by the same set of equations.

We require a numerical scheme to solve this problem, of which there are many

for conservation laws. Traditional schemes, such as Lax Wendroff and central difference, are unsplit (that is they take no account of the direction of flow). These schemes often inherently cause oscillations in space, near discontinuities. Since the 1980's, upwind schemes have become popular, since they are found to give better results for conservation laws, the main examples of these being Roe, Osher and Van Leer.

Roe's scheme has been tried in [1] for this problem, but the scheme is observed to give oscillations in time. In this work we investigate the cause of these oscillations, and attempt to alleviate the problem.

In chapter 2 we quote and describe the open channel equations, justify the use of the slot and set up the problem that forms the basis of this work.

The first thing we do after reproducing the results in [1], is to try some other upwind schemes in order to see what effect they have on the oscillations. This forms chapters 3 to 5.

The presence of the narrow slot causes a sharp jump in the characteristic waves speeds as we enter the slot. In chapter 6 we try two different ways of smoothing this jump to see what effect this has on the oscillations.

In chapter 7 we try an implicit version of Roe's scheme, and also alternatives to Euler time stepping.

In chapter 8 we develop a 'shock' fitting modification to Roe's scheme.

In chapter 9 we summarise the conclusions we have made from the proceeding chapters.

Chapter 2

Simulation of Pressurized Flow with the Open Channel Equations

2.1 The Open Channel Equations

The unsteady 1-D open channel equations, often referred to as the St. Venant equations, can, for a prismatic channel (i.e. constant cross-section), be written in conservation form as follows (see [12] pp. 451 or [2] pp. 7, for the derivation),

$$\frac{\partial \mathbf{w}}{\partial t} + \frac{\partial \mathbf{F}(\mathbf{w})}{\partial x} = \mathbf{D} \tag{2.1}$$

where

$$\mathbf{w} = \begin{bmatrix} A \\ Q \end{bmatrix}, \mathbf{F}(\mathbf{w}) = \begin{bmatrix} Q \\ \frac{Q^2}{A} + I_1(A) \end{bmatrix}, \mathbf{D} = \begin{bmatrix} 0 \\ gA(S_0 - S_f) \end{bmatrix}.$$

Equation (2.1) uses the following notation

h = water depth

$$
\begin{aligned}
Q &= \text{flow rate} \\
A &= \text{wetted cross-sectional area} \\
b &= \text{channel width at height } \eta \text{ above bottom} \\
S_0 &= \text{bottom slope} \\
S_f &= \text{friction slope} \\
g &= \text{gravitational acceleration} \\
I_1(A) &= \int_0^h g(h-\eta)b(\eta)d\eta.
\end{aligned}
$$

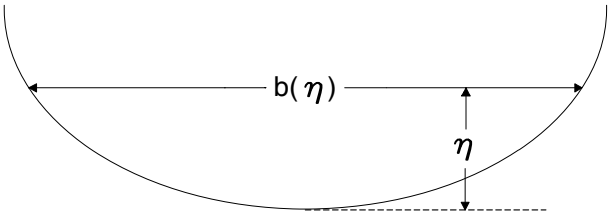

Figure 2.1: A typical channel cross-section.

We shall use Manning's formula to calculate the frictional resistance F_f (see [12] pp. 454-457),

$$F_f = \frac{\rho g A v|v|}{R^{4/3}} \left(\frac{n}{1.49}\right)^2$$

where

$$
\begin{aligned}
v &= \frac{Q}{A} \\
n &= \text{Manning's roughness coefficient} \\
R &= \text{hydraulic radius} \\
&= \frac{\text{wetted area}}{\text{wetted perimeter}}
\end{aligned}
$$

$$\rho \;=\; \text{density}$$

The friction slope S_f is defined by

$$S_f = \frac{1}{\rho g A} F_f$$

hence

$$S_f = \frac{v|v|}{R^{4/3}} \left(\frac{n}{1.49} \right)^2 \tag{2.2}$$

We can write equation (2.1) as

$$\frac{\partial \mathbf{w}}{\partial t} + J(\mathbf{w}) \frac{\partial \mathbf{w}}{\partial x} = \mathbf{D}$$

where J is the Jacobian of $\mathbf{F}$

$$J(\mathbf{w}) = \frac{\partial \mathbf{F}(\mathbf{w})}{\partial \mathbf{w}} = \begin{bmatrix} 0 & 1 \\ -\dfrac{Q^2}{A^2} + c^2 & \dfrac{2Q}{A} \end{bmatrix}$$

where

$$c^2 = \frac{d}{dA} I_1(A).$$

If $b(\eta)$ is continuous at $\eta = h$, then

$$\begin{aligned} c^2 = \frac{d}{dA} \int_0^h g(h-\eta) b(\eta) d\eta &= \frac{dh}{dA} \frac{d}{dh} \int_0^h g(h-\eta) b(\eta) d\eta \\ &= \frac{dh}{dA} \left(g \int_0^h b(\eta) d\eta + g(h-h) b(h) \right) \\ &= g \frac{dh}{dA} \int_0^h b(\eta) d\eta. \end{aligned}$$

From the definition of wetted area, we know that

$$A = \int_0^h b(\eta) d\eta$$

so

$$\frac{dA}{dh} = b(h) = b_s$$

where b_s is the channel width at the free surface; hence we have that

$$c^2 = \frac{gA}{b_s}. \tag{2.3}$$

Note that $J(\mathbf{w})$ has eigenvalues

$$\lambda_1 = \frac{Q}{A} - c \ , \ \lambda_2 = \frac{Q}{A} + c$$

and corresponding eigenvectors

$$\mathbf{e_1} = \begin{bmatrix} 1 \\ \\ \lambda_1 \end{bmatrix} \ , \ \mathbf{e_2} = \begin{bmatrix} 1 \\ \\ \lambda_2 \end{bmatrix}.$$

2.2 Simulation of Pressurized Flows

Equation (2.1) applies to flows in open channels, where there is a free surface. In a closed channel, while the water is below the soffit, we can continue to use the open channel equations as before. If part of the free surface reaches the soffit, then this portion of the flow will no longer have a free surface and hence will be pressurized. In this portion, the open channel equations will no longer be valid.

The major feature of pressurized flow is that it has an extremely large wave celerity c, compared to the wave celerity of free surface flow. This arises from the fact that when the flow is pressurized, there is no additional storage volume left; hence if the flow changes at the upstream end the effect is immediately transmitted downstream.

In order to simulate pressurized conditions using the open channel equations, we can add a narrow vertical slot in the channel soffit as shown in figure 2.2 (see [2] pp. 367).

While normal free surface conditions hold, the slot has no effect. When the flow is pressurized the free surface level is in the slot. Because the slot is very narrow, the volume of water it holds is negligible compared to the pipe volume, so the continuity equation still holds. We see from equation (2.3) that the small slot width, w_{sl}, produces a large celerity c. This large wave celerity is an attempt to approximate the very large wave celerity of pressurized flow. Hence, using the slot, we can simulate pressurized flow using the open channel equations. The slot has an infinite height.

The problem does not have an analytic solution, and hence a numerical approach is required. It is anticipated that the problem will cause numerical prob-

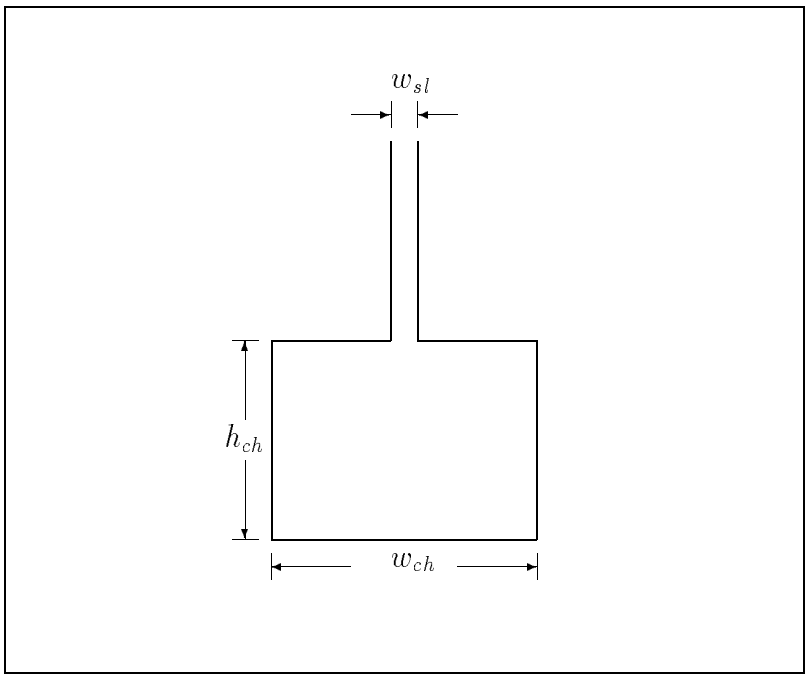

Figure 2.2: Rectangular channel with slot in soffit (slot width exaggerated)

lems, because of the sudden change in channel width as we enter the slot.

In the next section are the details of the particular problem that will form the basis for the whole of this dissertation.

2.3 Description of the Problem

The problem tackled in this work is from [1]. It consists of a rectangular channel, as in figure 2.2. The properties of the channel are given as follows,

$$\begin{aligned} \text{Channel width } (w_{ch}) &= 0.51\text{m} \\ \text{Channel height}(h_{ch}) &= 0.148\text{m} \\ \text{Channel length} &= 10\text{m} \\ \text{Channel slope} &= 0 \\ \text{Manning constant}(n) &= 0.012 \\ \text{Slot width}(w_{sl}) &= 0.01\text{m}. \end{aligned}$$

The following initial conditions are given

$$\begin{aligned} A(x,0) &= 0.06528 \text{ m}^2 \\ Q(x,0) &= 0 \text{ m}^3\text{s}^{-1}. \end{aligned}$$

The boundary conditions are given by the following data

At $x = 0$ (see figure 2.3)

Time (s)	Water depth (m)	Time (s)	Water depth (m)
0.0	0.1280	3.4	0.1728
0.2	0.1290	3.6	0.1752
0.4	0.1300	3.8	0.1778
0.6	0.1330	4.0	0.1800
0.8	0.1360	4.2	0.1830
1.0	0.1400	4.4	0.1870
1.2	0.1420	4.6	0.1900
1.4	0.1440	4.8	0.1920
1.6	0.1460	5.0	0.1920
1.8	0.1470	5.2	0.1916
2.0	0.1500	5.4	0.1896
2.2	0.1516	5.6	0.1880
2.4	0.1540	5.8	0.1880
2.6	0.1580	6.0	0.1888
2.8	0.1610	6.2	0.1908
3.0	0.1640	6.4	0.1948
3.2	0.1688	6.6	0.1972

At $x = 10.0$

Time (s)	Water depth (m)	Time (s)	Water depth (m)
0.0	0.1280	6.6	0.1280

Intermediate values are obtained by linear interpolation.

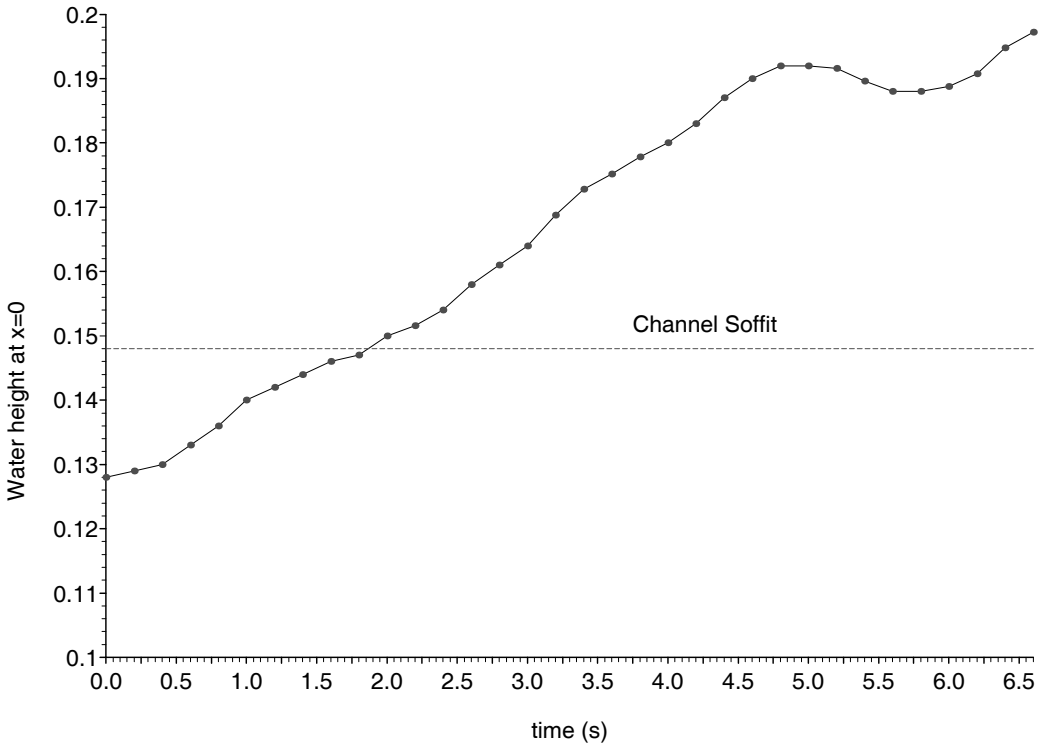

Figure 2.3: Water height at left boundary against time.

The main thing that we need to calculate for our problem, is the integral $I_1(A)$ (see equation (2.1)). This is given by the following formula

$$I_1(A) = \begin{cases} \dfrac{gA^2}{2w_{ch}} & A \leq A_{crit} \\ gA_{crit}\left(\dfrac{(A - A_{crit})}{w_{sl}} + \dfrac{h_{ch}}{2}\right) + \dfrac{g(A - A_{crit})^2}{2w_{sl}} & A > A_{crit} \end{cases}$$

where $A_{crit} = h_{ch}w_{ch}$.

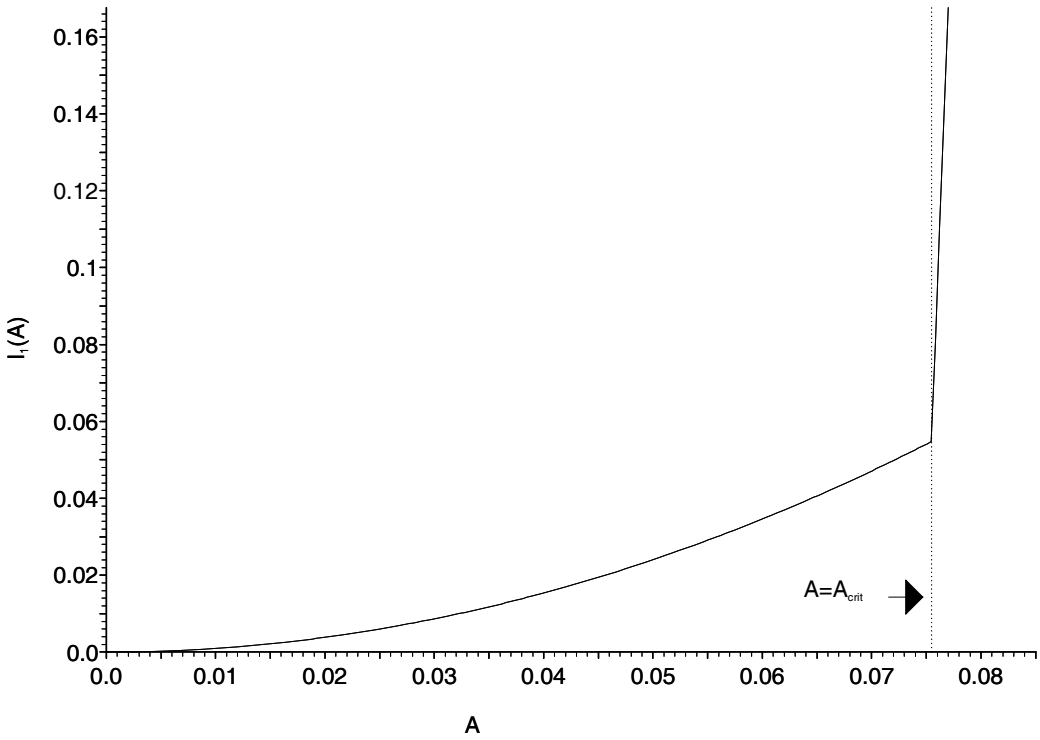

Figure 2.4: Plot of $I_1(A)$ for our channel.

I_1 (see figure 2.4) is a continuous function, and it is differentiable everywhere, except at $A = A_{crit}$. c is not strictly defined at this point, although we can take limits from above and below,

$$c_- = \left(\frac{gA_{crit}}{w_{ch}}\right)^{1/2}, \qquad c_+ = \left(\frac{gA_{crit}}{w_{sl}}\right)^{1/2}.$$

c (see figure 2.5) is then discontinuous at $A = A_{crit}$, and the jump is given by

$$\Delta c = c_+ - c_-.$$

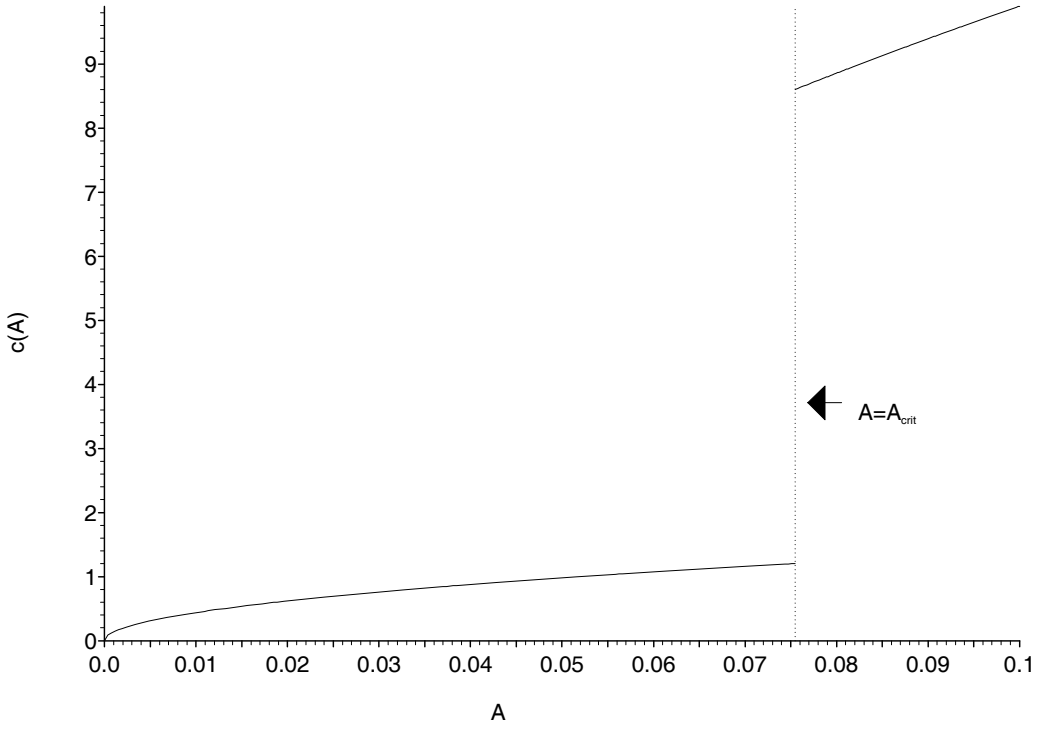

Figure 2.5: Plot of $c(A)$ for our channel.

Chapter 3

Roe's Scheme

3.1 Description of the Scheme

This scheme was originally developed for the Euler equations in [9]. In common with other schemes used in this work, we approximate the solution function $w(x)$, by a set of piecewise constant states $\{w_j\}$, of constant width Δx (see figure 3.1).

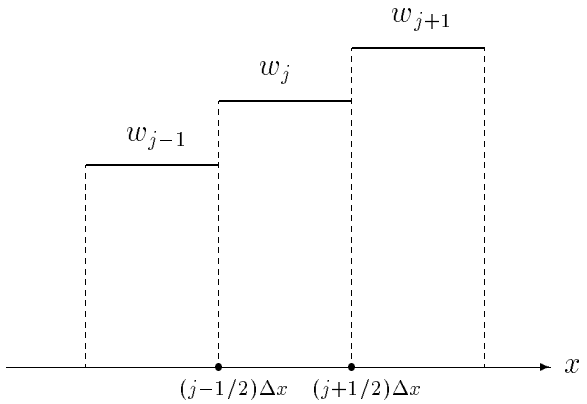

Figure 3.1: Piecewise constant states.

w_j is taken to be the cell average of the function w, on the interval

$$[(j-1/2)\Delta x, (j+1/2)\Delta x]$$

and is given by

$$w_j = \frac{1}{\Delta x} \int_{(j-1/2)\Delta x}^{(j+1/2)\Delta x} w(x)dx$$

This property ensures that the piecewise constant approximation has the 'same amount of w' as the original function.

Suppose $\{\mathbf{w}_j^n\}$ are the cell averages to some approximation of the exact solution of the PDE (2.1) with $\mathbf{D} = \mathbf{0}$, at $t = n\Delta t$. We then have a sequence of Riemann problems centred at $x = (j + 1/2)\Delta x, t = n\Delta t$, $j = 0, 1, \ldots$.

In Roe's scheme we approximate the Jacobian, $J(\mathbf{w})$, in the interval $[j\Delta x, (j + 1)\Delta x]$ by the constant matrix $\tilde{J}(\mathbf{w}_L, \mathbf{w}_R)$, where $\mathbf{w}_L = \mathbf{w}_j^n$ and $\mathbf{w}_R = \mathbf{w}_{j+1}^n$. We can then solve the Riemann problem exactly, with this new constant matrix (see below).

The matrix $\tilde{J}$ is chosen so to have the following three properties,

1. As $\mathbf{w}_L \to \mathbf{w}_R \to \mathbf{w}$

   $\tilde{J}(\mathbf{w}_L, \mathbf{w}_R) \to J(\mathbf{w})$

2. For any $\mathbf{w}_L, \mathbf{w}_R$

   $\tilde{J}(\mathbf{w}_L, \mathbf{w}_R)(\mathbf{w}_R - \mathbf{w}_L) = \mathbf{F}(\mathbf{w}_R) - \mathbf{F}(\mathbf{w}_L)$

3. The eigenvectors of $\tilde{J}$ are linearly independent.

These three properties ensure conservation, and that any shock will satisfy the Rankine-Hugoniot condition (See [9] for more details).

The matrix that has these properties is as follows,

$$\tilde{J}(\mathbf{w}_L, \mathbf{w}_R) = \begin{bmatrix} 0 & 1 \\ -\dfrac{\tilde{Q}^2}{\tilde{A}^2} + \tilde{c}^2 & \dfrac{2\tilde{Q}}{\tilde{A}} \end{bmatrix}$$

where

$$\tilde{A} = (A_L A_R)^{1/2}$$

$$\tilde{Q} = \frac{(A_L)^{1/2} Q_R + (A_R)^{1/2} Q_L}{(A_L)^{1/2} + (A_R)^{1/2}}$$

$$\tilde{c} = \begin{cases} \left[\dfrac{I_1(A_R) - I_1(A_L)}{A_R - A_L} \right]^{1/2} & A_R - A_L \neq 0 \\ \\ \left[\dfrac{g(A_R + A_L)}{(b_s)_R + (b_s)_L} \right]^{1/2} & A_R - A_L = 0 \end{cases}$$

$\tilde{J}$ has eigenvalues

$$\tilde{\lambda}_1 = \frac{\tilde{Q}}{\tilde{A}} - \tilde{c} \ , \ \tilde{\lambda}_2 = \frac{\tilde{Q}}{\tilde{A}} + \tilde{c}$$

and corresponding eigenvectors

$$\tilde{\mathbf{e}}_\mathbf{1} = \begin{bmatrix} 1 \\ \\ \tilde{\lambda}_1 \end{bmatrix} \ , \ \tilde{\mathbf{e}}_\mathbf{2} = \begin{bmatrix} 1 \\ \\ \tilde{\lambda}_2 \end{bmatrix}.$$

If we decompose the jumps in $\mathbf{w}$ as follows (see [9])

$$\mathbf{w}_R - \mathbf{w}_L = \tilde{\alpha}_1 \tilde{\mathbf{e}}_1 + \tilde{\alpha}_2 \tilde{\mathbf{e}}_2$$

then using the properties of the matrix $\tilde{J}$ the flux difference is

$$\mathbf{F}(\mathbf{w}_R) - \mathbf{F}(\mathbf{w}_L) = \tilde{\lambda}_1 \tilde{\alpha}_1 \tilde{\mathbf{e}}_1 + \tilde{\lambda}_2 \tilde{\alpha}_2 \tilde{\mathbf{e}}_2.$$

Here $\tilde{\alpha}_1$ and $\tilde{\alpha}_2$ are found to be the strengths of the waves corresponding to the eigenvectors $\tilde{\mathbf{e}}_1$ and $\tilde{\mathbf{e}}_2$, respectively, and are found to be

$$\tilde{\alpha}_1 = \frac{\tilde{\lambda}_2 (A_R - A_L) - (Q_R - Q_L)}{\tilde{\lambda}_2 - \tilde{\lambda}_1}$$

$$\tilde{\alpha}_2 = \frac{(Q_R - Q_L) - \tilde{\lambda}_1 (A_R - A_L)}{\tilde{\lambda}_2 - \tilde{\lambda}_1}$$

The source term $\mathbf{D}$ in (2.1) can also be decomposed onto the eigenvectors as follows

$$\tilde{\mathbf{D}} = \tilde{\beta}_1 \tilde{\mathbf{e}}_1 + \tilde{\beta}_2 \tilde{\mathbf{e}}_2$$

where $\tilde{\mathbf{D}}$ is some average of $\mathbf{D}_L$ and $\mathbf{D}_R$, which are the source terms on the left and right. This work uses $\tilde{\mathbf{D}} = \frac{1}{2}(\mathbf{D}_L + \mathbf{D}_R)$. If $\tilde{\mathbf{D}} = [0, \tilde{D}]^T$ then

$$\begin{aligned} \tilde{\beta}_1 &= \frac{-\tilde{D}}{\tilde{\lambda}_2 - \tilde{\lambda}_1} \\ \tilde{\beta}_2 &= -\tilde{\beta}_1. \end{aligned}$$

We now get to the main part of the algorithm.

Suppose we have $N+1$ constant states altogether, then we will have N Riemann problems. For the j^{th} Riemann problem centred at $x = (j+1/2)\Delta x$ we calculate and keep the following

$$\left.\begin{aligned} &\tilde{\lambda}_{i,j+1/2} = \tilde{\lambda}_i \\ &\mathbf{\Phi}_{i,j+1/2} = \left(-\frac{\Delta t}{\Delta x}\tilde{\lambda}_i\tilde{\alpha}_i + \Delta t\tilde{\beta}_i\right)\tilde{\mathbf{e}}_i \end{aligned}\right\} i = 1, 2$$

The terms $\mathbf{\Phi}_{i,j+1/2}$ are the time updates to the components of $\mathbf{w}$ (corresponding to $\tilde{\mathbf{e}}_1$ and $\tilde{\mathbf{e}}_2$) using an explicit Euler scheme. This is carried out for $j = 0, 1, \ldots, N-1$.

We now use the following procedure to update the solution to the next time level.

For $j = 0, 1, \ldots, N-1$

$$\left.\begin{aligned} &\text{if } \tilde{\lambda}_{i,j+1/2} > 0 \text{ then increment } \mathbf{w}_{j+1} \text{ by } \mathbf{\Phi}_{i,j+1/2}, \\ &\text{else increment } \mathbf{w}_j \text{ by } \mathbf{\Phi}_{i,j+1/2}. \end{aligned}\right\} i = 1, 2$$

Figure 3.2 shows the transfers for one possible case. The solution is now updated except for the updates due to the boundary conditions, which will be discussed later. We need the CFL condition

$$\max(|\tilde{\lambda}_{1,j+1/2}|, |\tilde{\lambda}_{2,j+1/2}|)\frac{\Delta t}{\Delta x} \leq 1$$

to ensure that neighbouring Riemann problems do not interact.

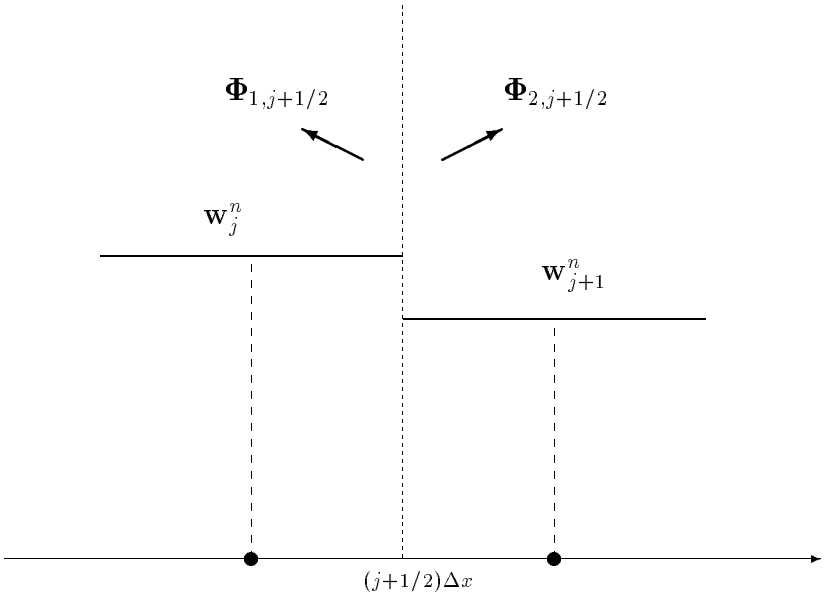

Figure 3.2: Transfer across interface at $x = (j + 1/2)\Delta x$, if $\tilde{\lambda}_{1,j+1/2} \leq 0$ and $\tilde{\lambda}_{2,j+1/2} > 0$.

The resulting scheme is first order in space and time. The scheme can be made second order, by transferring a proportion of the flux ($\mathbf{\Phi}_{i,j+1/2}$) back in the opposite direction. The proportion is controlled by a limiter, which can be chosen to ensure second order accuracy whilst keeping shocks sharp and free of oscillations (see [3] and [8]). The results in this project do not use a limiter however.

At boundaries the wave-like nature of the decomposed variables is exploited, so that only incoming waves are updated from the appropriate boundary condition. Outgoing waves are allowed to pass freely from the region. If at a boundary both waves move into the region, then two boundary conditions are required in order to overwrite both characteristic variables. If however only one wave is incoming

at a boundary, then it is only appropriate to overwrite the incoming characteristic variable, hence we must have only one boundary condition.

The only case encountered in this work is where we have only one incoming wave at each end, and we wish to specify the height of the water at the boundaries for each time step. We can directly overwrite the area variable, A, with the new area (calculated from the new height), but we do not know what to do with the Q variable. This problem can be solved by extrapolating from the interior values near the boundary, an incoming wave at the boundary. The strength of this wave is chosen so as to give the correct value of A at the boundary. This wave is then used to increment the Q value at the boundary. See [3] for details.

In rare situations Roe's scheme can give unphysical solutions, i.e. entropy violating. The solution can have a shock, when the correct entropy satisfying solution has an expansion fan. A modification to the scheme is available to ensure that solutions do not violate the entropy condition. This modification was not needed in this work. See [3] for details.

3.2 Results and Discussion

Figure 3.3 shows water height against distance along the channel, at several different times. Before the surface reaches the slot, the numerical solution is smooth and well behaved. After the surface goes into the slot, a sharp front develops which separates the pressurized flow from the free surface flow. This front is shock-like, but is not a shock. A low frequency oscillation develops behind this front, which however does not appear too serious.

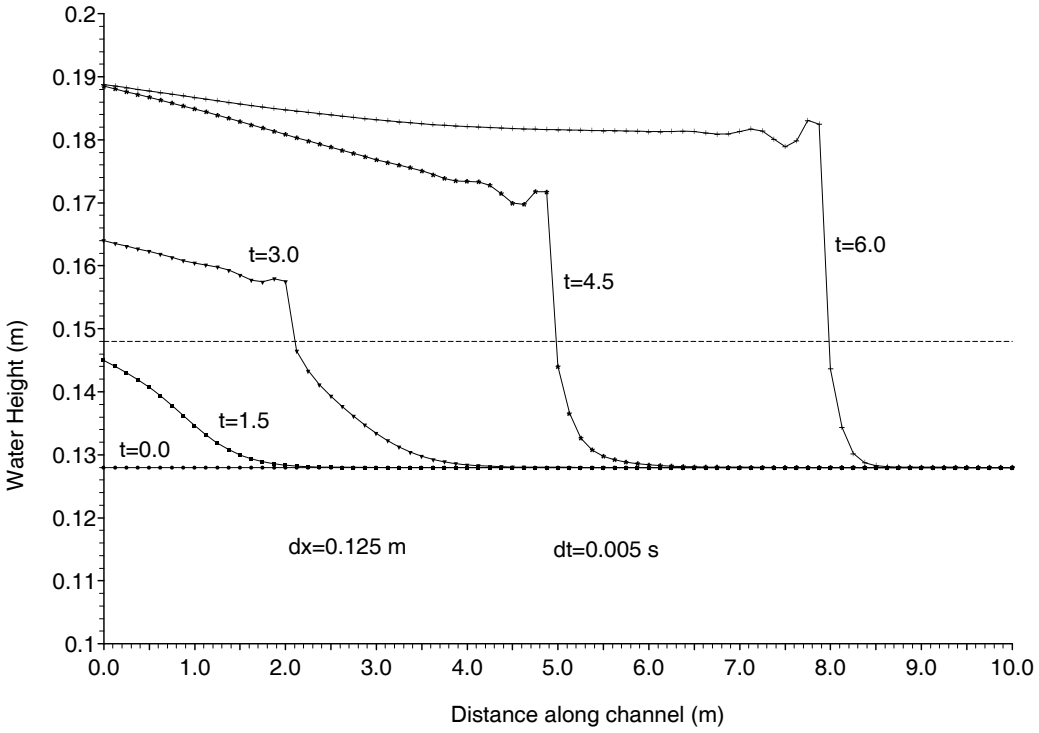

Figure 3.3: Water height against distance along channel, at several different times.

The problem occurs when we look at a time history of the water height, at a particular distance along the channel. Figure 3.4 shows such a history at distance 3.5m. The water height initially remains constant, and then rises smoothly until it reaches the slot. It then rises very sharply into the slot; after this there is

a series of high frequency oscillations, which eventually decay and the height returns to smooth variation. The oscillations are the ones observed in [1] which prompted this work.

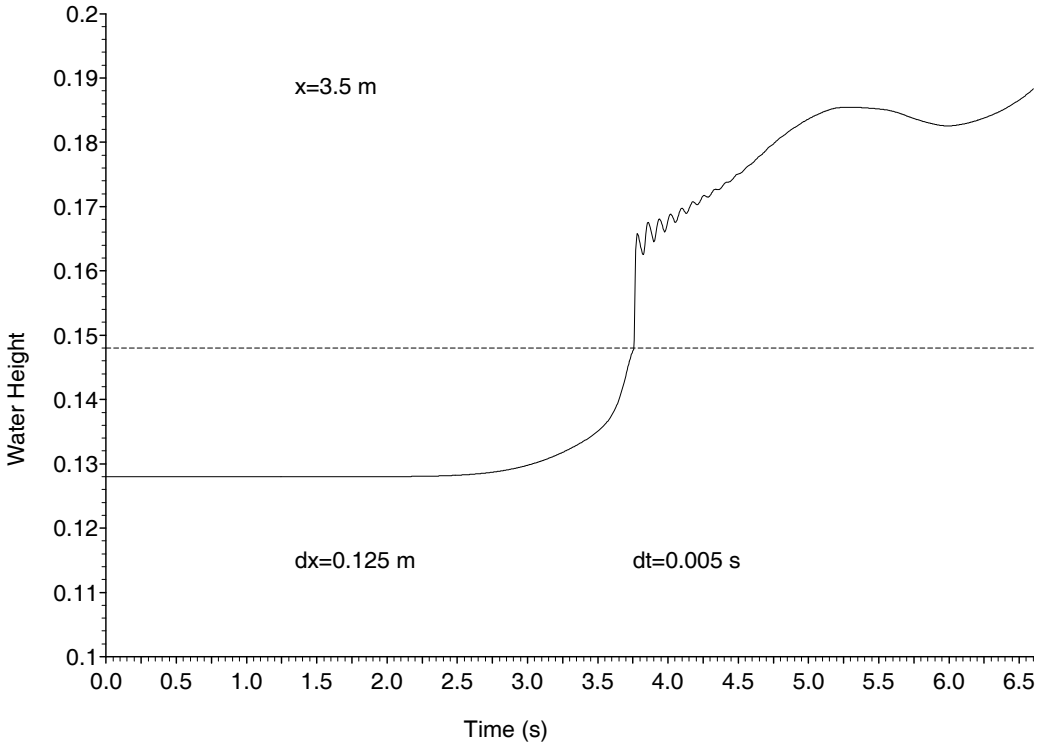

Figure 3.4: Water height against time, at 3.5m along channel.

The most obvious explanation for the oscillations is the discontinuity in the wave celerity, which causes a discontinuity in the characteristic wave speeds (see Figure 2.5). Of course, the scheme cannot resolve this discontinuity, but sees a sharp change in wave speeds as the surface enters the slot. Another problem could be the piece-wise constant approximation, because near the front the solution does not vary smoothly; hence this approximation can become a poor one. The source term could be a cause, but this can practically be ruled out since the oscillations are still present, even for the homogeneous problem.

When the grid is made finer and a smaller time step is used (in order to satisfy

the CFL condition), we observe that the the oscillations increase in frequency and decay at a faster rate. This can be seen from figure 3.5.

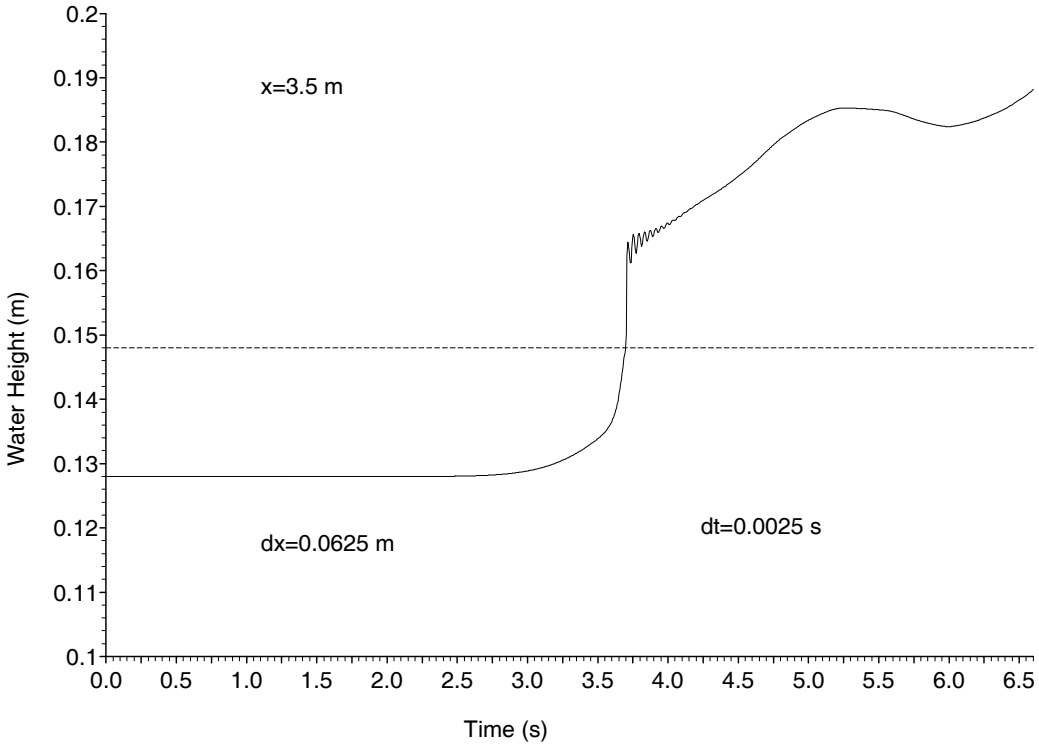

Figure 3.5: Water height against time, using a finer grid.

In Roe's scheme we are basically making two approximations,

- Solving each Riemann problem in a approximate manner.
- Re-averaging the solutions to recover piece-wise constant states.

In Roe's scheme, we obtain an approximate solution to each Riemann problem by assuming that the characteristic speeds are constant; we take some kind of average for these constant values. This could be the problem, since the characteristic speeds do not vary smoothly near the pressurized/free surface interface. This hypothesis can be tested, by trying other approximate Riemann solvers which

can, perhaps, take account of the sharp variation in a better way. This will be our next task.

Chapter 4

The Osher and Solomon Scheme

This scheme was used, in order to see if the oscillations observed with Roe's scheme are a peculiarity of Roe's scheme, or whether other schemes suffer from them. See [7] for much more detail on the scheme.

4.1 Description of the Scheme [7]

The Osher and Solomon scheme is the Engquist-Osher scheme generalised to systems. For the scalar conservation law

$$\frac{\partial w}{\partial t} + \frac{\partial f(w)}{\partial x} = 0, \; w(x,0) = \phi(x)$$

the Engquist-Osher scheme is as follows

$$w_j^{n+1} = w_j^n - \frac{\Delta t}{\Delta x}(f_-(w_{j+1}^n) - f_-(w_j^n) + f_+(w_j^n) - f_+(w_{j-1}^n))$$

$$w_j^0 = \phi(j\Delta x)$$

Here

$$f_+(u) = \int_0^u \chi(s) f'(s) ds$$

$$f_-(u) = \int_0^u (1-\chi(s))f'(s)ds$$

where

$$\chi(u) = 1 \quad \Leftrightarrow \quad f'(u) > 0$$

$$\chi(u) = 0 \quad \Leftrightarrow \quad f'(u) \leq 0.$$

We can also write the scheme as follows

$$w_j^{n+1} = w_j^n - \frac{\Delta t}{\Delta x}\left(\int_{w_{j-1}^n}^{w_j^n} \chi(w)f'(w)dw + \int_{w_j^n}^{w_{j+1}^n}(1-\chi(w))f'(w)dw\right)$$

This can be extended to a system in the following way

$$\mathbf{w}_j^{n+1} = \mathbf{w}_j^n - \frac{\Delta t}{\Delta x}\left(\int_{\mathbf{w}_{j-1}^n}^{\mathbf{w}_j^n} \chi(\mathbf{w})J(\mathbf{w})\mathbf{dw} + \int_{\mathbf{w}_j^n}^{\mathbf{w}_{j+1}^n}(I-\chi(\mathbf{w}))J(\mathbf{w})\mathbf{dw}\right)$$

where J is the Jacobian and χ is some matrix that needs to be chosen. We also need to choose the paths of integration.

Let the eigenvalues of J be denoted by $\lambda_1(\mathbf{w}) < \lambda_2(\mathbf{w}) < \ldots < \lambda_m(\mathbf{w})$ with corresponding eigenvectors $\mathbf{e}_1(\mathbf{w}), \mathbf{e}_2(\mathbf{w}), \ldots, \mathbf{e}_m(\mathbf{w})$. Let $T(\mathbf{w})$ be the matrix whose j^{th} column is $\mathbf{e}_j(\mathbf{w})$, then we have that

$$T^{-1}(\mathbf{w})J(\mathbf{w})T(\mathbf{w}) = \text{diag}\{\lambda_k(\mathbf{w})\}.$$

Defining $\chi(\mathbf{w})$ by

$$\chi(\mathbf{w}) = \frac{1}{2}T(\mathbf{w})\text{diag}\{1+\text{sign}(\lambda_k(\mathbf{w}))\}T^{-1}(\mathbf{w})$$

we have

$$\begin{aligned}\chi(\mathbf{w})J(\mathbf{w}) &= T(\mathbf{w})\text{diag}\{\max(\lambda_k(\mathbf{w}),0)\}T^{-1}(\mathbf{w}) &= J^+(\mathbf{w})\\ (I-\chi(\mathbf{w}))J(\mathbf{w}) &= T(\mathbf{w})\text{diag}\{\min(\lambda_k(\mathbf{w}),0)\}T^{-1}(\mathbf{w}) &= J^-(\mathbf{w})\end{aligned}$$

If Γ^j is the path connecting $\mathbf{w}_{j-1}$ *to* $\mathbf{w}_j$, then we decompose this curve into m sub-curves

$$\Gamma^j = \bigcup_{k=1}^m \Gamma_k^j.$$

These sub-curves are related to rarefaction or compression wave solutions and are defined by

$$\Gamma_k^j = \begin{cases} \dfrac{d\mathbf{w}^{(k)}}{ds} = \mathbf{e}_k & \text{for either } 0 \le s \le s_k^{(j)} \text{ or } 0 \ge s \ge s_k^{(j)} \\ \mathbf{w}^{(k)}(0) = \mathbf{w}^{(k+1)}(s_{k+1}^{(j)}) \end{cases}$$

with

$$\mathbf{w}^{(m+1)}(s_{m+1}^{(j)}) = \mathbf{w}_{j-1} \text{ and } \mathbf{w}^{(1)}(s_1^{(j)}) = \mathbf{w}_j.$$

The scheme can now be written as

$$\mathbf{w}_j^{n+1} = \mathbf{w}_j^n - \frac{\Delta t}{\Delta x}\left[\sum_{k=1}^{m}\left(\int_{\Gamma_k^j} J^+(\mathbf{w})\mathbf{dw} + \int_{\Gamma_k^{j+1}} J^-(\mathbf{w})\mathbf{dw}\right)\right]$$

If the k^{th} field is genuinely non-linear, it turns out that (see [7])

$$\int_{\Gamma_k^j} J^+(\mathbf{w})\mathbf{dw} = \begin{cases} \mathbf{F}(\mathbf{w}^{(k-1)}(0)) - \mathbf{F}(\mathbf{w}^{(k)}(0)) & \text{if } \lambda_k^- > 0 \ \& \ \lambda_k^+ > 0 \\ \mathbf{F}(\mathbf{w}^{(k-1)}(0)) - \mathbf{F}(\bar{\mathbf{w}}_j^k) & \text{if } \lambda_k^- > 0 \ \& \ \lambda_k^+ \le 0 \\ \mathbf{F}(\bar{\mathbf{w}}_j^k) - \mathbf{F}(\mathbf{w}^{(k)}(0)) & \text{if } \lambda_k^- \le 0 \ \& \ \lambda_k^+ > 0 \\ 0 & \text{if } \lambda_k^- \le 0 \ \& \ \lambda_k^+ \le 0 \end{cases}$$

and

$$\int_{\Gamma_k^j} J^-(\mathbf{w})\mathbf{dw} = \begin{cases} \mathbf{F}(\mathbf{w}^{(k-1)}(0)) - \mathbf{F}(\mathbf{w}^{(k)}(0)) & \text{if } \lambda_k^- \le 0 \ \& \ \lambda_k^+ \le 0 \\ \mathbf{F}(\mathbf{w}^{(k-1)}(0)) - \mathbf{F}(\bar{\mathbf{w}}_j^k) & \text{if } \lambda_k^- \le 0 \ \& \ \lambda_k^+ > 0 \\ \mathbf{F}(\bar{\mathbf{w}}_j^k) - \mathbf{F}(\mathbf{w}^{(k)}(0)) & \text{if } \lambda_k^- > 0 \ \& \ \lambda_k^+ \le 0 \\ 0 & \text{if } \lambda_k^- > 0 \ \& \ \lambda_k^+ > 0 \end{cases}$$

where $\lambda_k^+ = \lambda_k(\mathbf{w}^{(k)}(0))$ and $\lambda_k^- = \lambda_k(\mathbf{w}^{(k-1)}(0))$. There exists at most one point $\bar{s}_k^{(j)}$ at which $\lambda_k(\mathbf{w}^{(k)}(\bar{s}_k^{(j)})) = 0$. Call this point $\bar{\mathbf{w}}_j^k = \mathbf{w}^{(k)}(\bar{s}_k^{(j)})$, a sonic point.

4.2 Scheme for Open Channel Equations

We return now to the open channel equations for which $m = 2$. Both fields are genuinely nonlinear, so we can use the above to calculate the integrals. Γ_1^j is

given by

$$A^1(s) = A^2(s_2^{(j)}) + s$$

$$Q^1(s) = (A^2(s_2^{(j)}) + s)\left[-\int_0^s \frac{c(A^2(s_2^{(j)}) + \eta)}{A^2(s_2^{(j)}) + \eta} d\eta + \frac{Q^2(s_2^{(j)})}{A^2(s_2^{(j)})}\right]$$

Γ_2^j is given by

$$A^2(s) = A_{j-1} + s$$

$$Q^2(s) = (A_{j-1} + s)\left[\int_0^s \frac{c(A_{j-1}) + \eta)}{A_{j-1} + \eta} d\eta + \frac{Q_{j-1}}{A_{j-1}}\right]$$

Using $A^1(s_1^{(j)}) = A_j$ and $Q^1(s_1^{(j)}) = Q_j$, we can find an explicit, but long equation for s_2^j in terms of A_{j-1}, Q_{j-1}, A_j and Q_j. It is now very straightforward to apply the scheme. We need the CFL condition

$$\max(|\lambda_1|, |\lambda_2|)\frac{\Delta t}{\Delta x} \leq 1$$

to ensure that neighbouring Riemann problems do not interact.

For this scheme it is best to implement the source terms in a pointwise manner, i.e.

$$\mathbf{w}_j^{n+1} = \mathbf{w}_j^n - \frac{\Delta t}{\Delta x}\left[\sum_{k=1}^m \left(\int_{\Gamma_k^j} J^+(\mathbf{w})\mathbf{dw} + \int_{\Gamma_k^{j+1}} J^-(\mathbf{w})\mathbf{dw}\right)\right] + \mathbf{D}(\mathbf{w}_j^n)\Delta t.$$

Implementing boundary conditions is more difficult for this scheme than for Roe's scheme. The crude way that was used for this work was as follows. At the boundary use only the valid part of the scheme. E.g. at the left hand boundary

$$\mathbf{w}_0^{n+1} = \mathbf{w}_0^n - \frac{\Delta t}{\Delta x}\left[\sum_{k=1}^m \left(\int_{\Gamma_k^1} J^-(\mathbf{w})\mathbf{dw}\right)\right] + \mathbf{D}(\mathbf{w}_0^n)\Delta t.$$

The new value of A_0^{n+1} is then directly written in.

Unlike Roe's scheme, all solutions given by the Osher and Solomon scheme are entropy satisfying (see [7]).

4.3 Results and Discussion

The Osher and Solomon scheme solves each Riemann problem approximately, but in a different way to Roe. This could have some effect on the oscillations, and in fact it does. This can be seen from figure 4.1, which shows a comparison of the results from this scheme against those from Roe. The oscillations are considerably larger than those from Roe; this was not expected, because the scheme's approximate Riemann solver is more elaborate than that of Roe, and should take better account of the sharp variation of the characteristic wave speeds near the front.

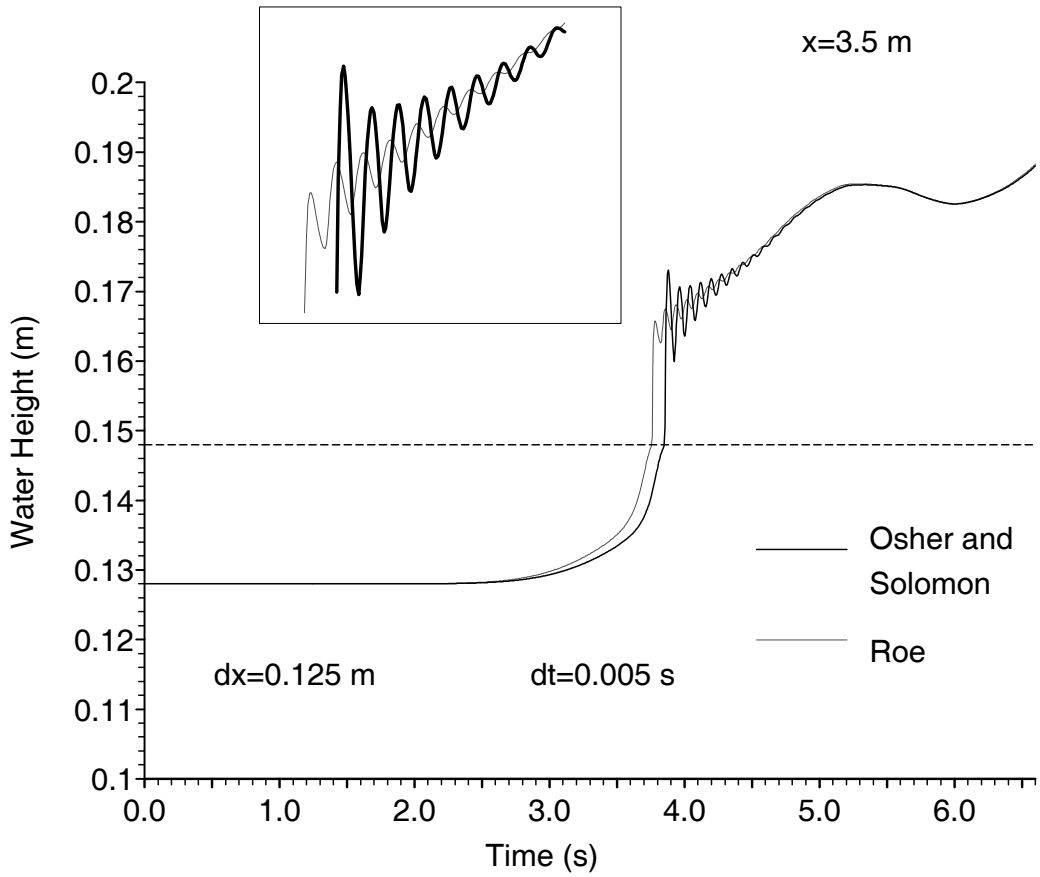

Figure 4.1: Comparison of results from Osher & Solomon against those from Roe.

The next step is to go one better, and solve each Riemann problem exactly before we re-average.

Chapter 5

Godunov's Scheme

After observing that both Roe's scheme and the Osher and Solomon scheme both suffer from the oscillations, the following question must be asked; are the oscillations due to the approximate nature of the Riemann solvers? This was tested by using the exact Riemann solver, i.e. using Godunov's method.

5.1 The Exact Riemann Solver for the Open Channel Equations

The Riemann problem

$$\frac{\partial \mathbf{w}}{\partial \mathrm{t}} + \frac{\partial \mathbf{F}(\mathbf{w})}{\partial x} = 0$$

$$\mathbf{w}(x,0) = \begin{cases} \mathbf{w}_L & \text{if} \quad x < 0 \\ \mathbf{w}_R & \text{if} \quad x > 0 \end{cases}$$

has a solution which just depends on the ratio x/t. Call it $\mathbf{w}^{(R)}(x/t, \mathbf{w}_L, \mathbf{w}_R)$. The solution is given by two waves of different speeds, separated by a constant state. Each of these waves will either be a shock wave or a rarefaction wave

(see [11]). Let us define the following curves in the (A, Q) plane,

$$\Gamma_1(\mathbf{w}_0) = \{(A,Q); A \geq 0, v + h(A) = v_0 + h(A_0)\}$$

$$\Gamma_2(\mathbf{w}_0) = \{(A,Q); A \geq 0, v - h(A) = v_0 - h(A_0)\}$$

$$S_1(\mathbf{w}_0) = \left\{(A,Q); A \geq 0, v = v_0 - (A - A_0)\left[\frac{I_1(A) - I_1(A_0)}{(A - A_0)AA_0}\right]^{1/2}\right\}$$

$$S_2(\mathbf{w}_0) = \left\{(A,Q); A \geq 0, v = v_0 + (A - A_0)\left[\frac{I_1(A) - I_1(A_0)}{(A - A_0)AA_0}\right]^{1/2}\right\}.$$

$$v = \frac{Q}{A}, \ , v_0 = \frac{Q_0}{A_0} \text{ and } h(A) = \int_{A^\star}^{A} \frac{c(s)}{s} ds$$

$A^\star \geq 0$ is some arbitrary reference state.

$\Sigma_1(\mathbf{w}_0)$ represents the states $\mathbf{w}$ that can be connected to $\mathbf{w}_0$ on the right by either a 1-shock or a 1-rarefaction. $\Sigma_2(\mathbf{w}_0)$ represents the states $\mathbf{w}$ that can be connected to $\mathbf{w}_0$ on the left by either a 2-shock or a 2-rarefaction (see [13] for more details)

$$\Sigma_1(\mathbf{w}_0) = \{\mathbf{w}; A \geq 0, \mathbf{w} \in \Gamma_1(\mathbf{w}_0) \text{ if } A \leq A_0; \mathbf{w} \in S_1(\mathbf{w}_0) \text{ if } A > A_0\}$$

$$\Sigma_2(\mathbf{w}_0) = \{\mathbf{w}; A \geq 0, \mathbf{w} \in \Gamma_2(\mathbf{w}_0) \text{ if } A \leq A_0; \mathbf{w} \in S_2(\mathbf{w}_0) \text{ if } A > A_0\}$$

If we solve exactly each Riemann problem, and then calculate the cell averages at the new time level, we get the Godunov scheme

$$\mathbf{w}_j^{n+1} = \mathbf{w}_J^n - \frac{\Delta t}{\Delta x}(\mathbf{F}(\mathbf{w}_{j+1/2}^{(R)}) - \mathbf{F}(\mathbf{w}_{j-1/2}^{(R)}))$$

where $\mathbf{w}_{j+1/2}^{(R)} = \mathbf{w}^{(R)}(0, \mathbf{w}_j^n, \mathbf{w}_{j+1}^n)$.

We need the CFL condition

$$\max(|\lambda_1|, |\lambda_2|)\frac{\Delta t}{\Delta x} \leq 1$$

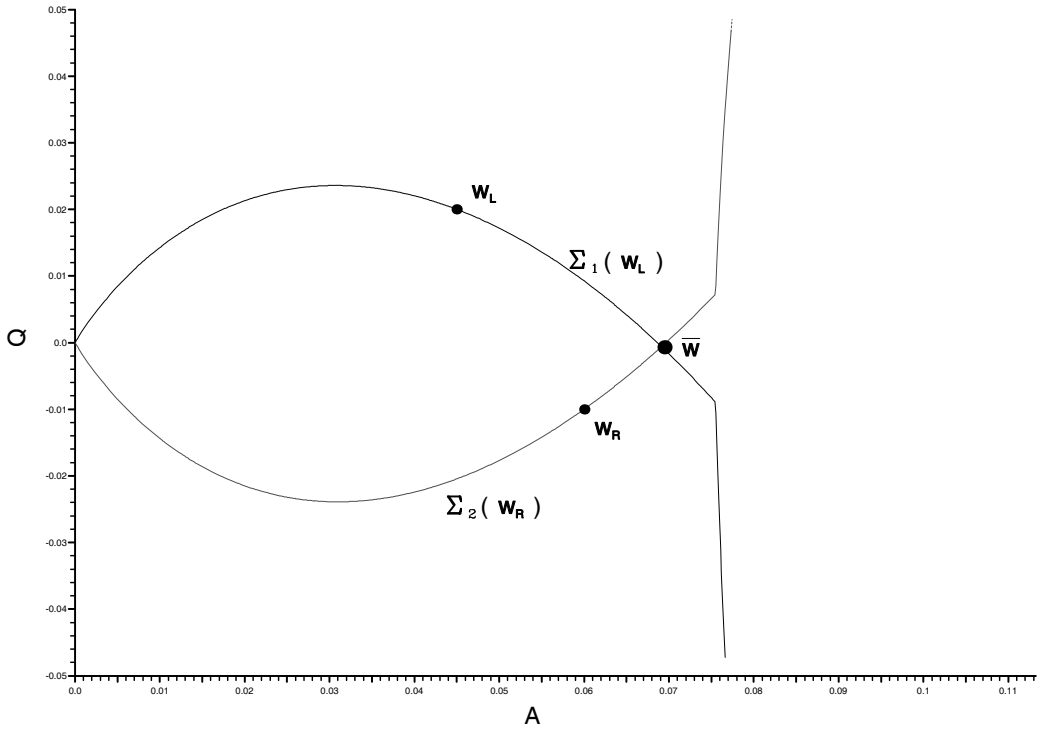

Figure 5.1: Riemann curves.

to ensure that neighbouring Riemann problems do not interact. See [4] , [3] pp. 56 and [5] pp. 444.

The following algorithm calculates $\mathbf{w}_s = \mathbf{w}^{(R)}(0, \mathbf{w}_L, \mathbf{w}_R)$ (see [13]).

$$\mathbf{w}_s = \mathbf{w}_L \begin{cases} \text{if} \quad \bar{A} \leq A_L \quad \text{and} \quad \lambda_1(\mathbf{w}_L) \geq 0, \\ \quad \text{or} \\ \text{if} \quad \bar{A} \geq A_L \quad \text{and} \quad \bar{Q} \geq Q_L, \end{cases}$$

$$\mathbf{w}_s = \mathbf{w}_R \begin{cases} \text{if} \quad \bar{A} \leq A_R \quad \text{and} \quad \lambda_2(\mathbf{w}_R) \leq 0, \\ \quad \text{or} \\ \text{if} \quad \bar{A} \geq A_R \quad \text{and} \quad \bar{Q} \leq Q_R, \end{cases}$$

$$\mathbf{w}_s = \Gamma_1(\mathbf{w}_L) \cap \{\lambda_1 = 0\} \quad \text{if } \lambda_1(\mathbf{w}_L) < 0 \leq \lambda_1(\bar{\mathbf{w}}),$$

$$\mathbf{w}_s = \Gamma_2(\mathbf{w}_R) \cap \{\lambda_2 = 0\} \quad \text{if } \lambda_2(\bar{\mathbf{w}}) < 0 \leq \lambda_2(\mathbf{w}_R),$$

$$\mathbf{w}_s = \bar{\mathbf{w}} \qquad \text{in other cases.}$$

$\bar{\mathbf{w}}$ is given by the non-trivial intersection of $\Sigma_1(\mathbf{w}_L)$ and $\Sigma_2(\mathbf{w}_R)$ (see figure 5.1). This is the constant state in the solution of the Riemann problem. A non-linear equation needs to be solved, in order to calculate $\bar{\mathbf{w}}$.

The source term $\mathbf{D}$ is implemented in a pointwise manner, the same as in the Osher and Solomon scheme.

The boundary conditions are implemented by calculating an imaginary state $\mathbf{w}^\star$ next to the boundary (outside region) such that, when using the scheme on the boundary, it results in the correct value being given to A.

5.2 Results and Discussion

In Godunov's scheme we are solving each Riemann problem exactly, before we re-average. This process is much more time consuming than the previous two schemes. Any errors that come from this scheme are due solely to the re-averaging process. Figure 5.2 shows results for Godunov, against those from Roe. There is a slight improvement in the oscillations; the first oscillation has a smaller amplitude.

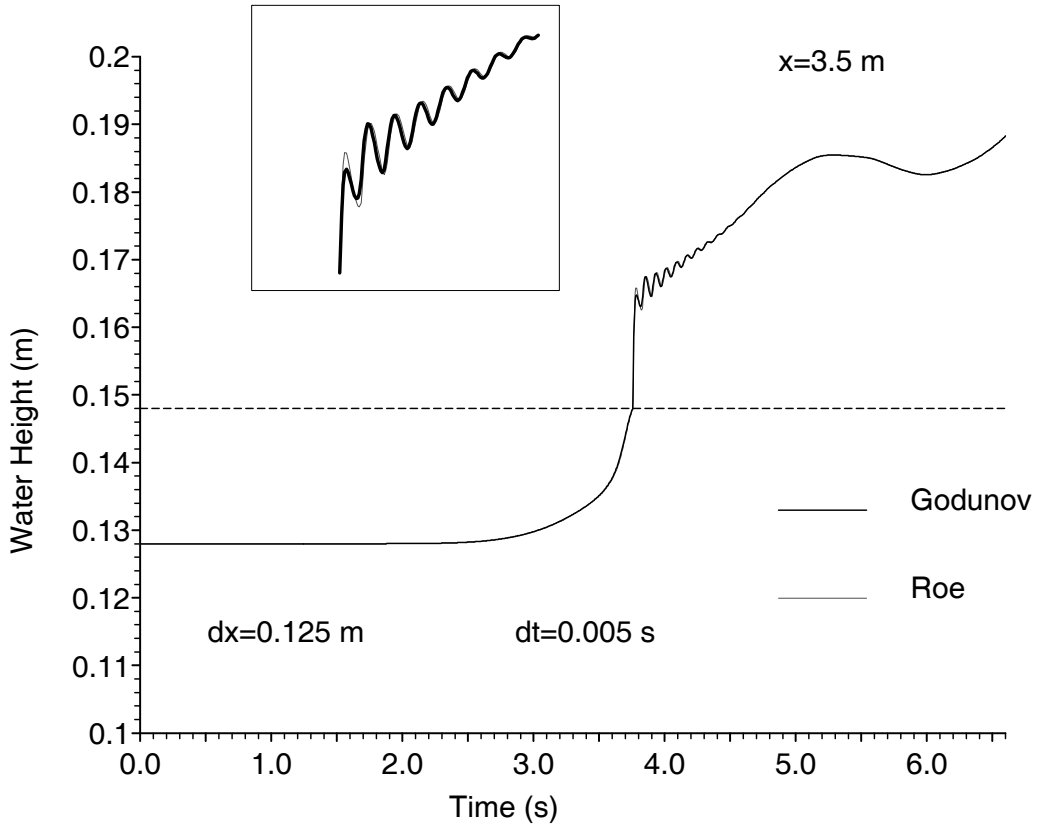

Figure 5.2: Comparison of results from Godunov against those from Roe.

These results indicate that it is not the approximate Riemann solvers that are to blame, but the re-averaging process; hence we are unlikely to improve the situation by solely modifying the Riemann solvers while keeping piecewise constant states.

Chapter 6

Smoothing Techniques

6.1 Smoothing Eigenvalues

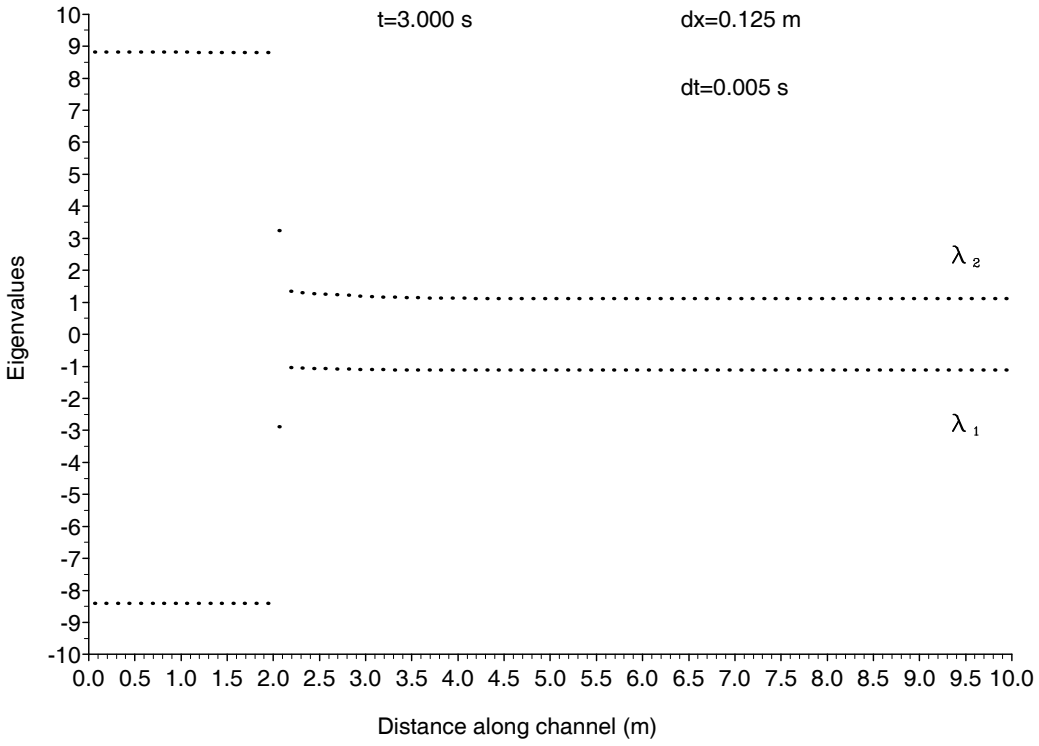

Figure 6.1: Eigenvalues from Roe's scheme.

Figure 6.1 is a plot of the sets of eigenvalues,$\{\lambda_{1,j+1/2}\}, \{\lambda_{2,j+1/2}\}$ from Roe's scheme. The sharp change in the eigenvalues occurs where the flow changes from being above the soffit to below it. It was thought that these sharp jumps were the cause of the oscillations. To test this, the eigenvalues were processed, after being calculated, so as to reduce the sharpness of the jump. These new sets of eigenvalues,$\{\lambda^{\star}_{1,j+1/2}\}, \{\lambda^{\star}_{2,j+1/2}\}$, were then used in the calculation of all further quantities. The 'smoothing' process was carried out for each time step, and in the following way,

$$\lambda^{\star}_{i,j+1/2} = \lambda_{i,j+1/2} + \epsilon \Delta t \delta^2_{j+1/2} \lambda_{i,j+1/2}$$

$i = 1, 2$ and $j = 1, \ldots\ldots, N-2$, where

$$\delta^2_{j+1/2} \lambda_{i,j+1/2} = \frac{\lambda_{i,j-1/2} - 2\lambda_{i,j+1/2} + \lambda_{i,j+3/2}}{\Delta x^2}$$

and ϵ is a free parameter.

6.1.1 Results and Discussion

Figure 6.2 shows the modified eigenvalues, at the same time as in figure 6.1. These have been generated from the modified scheme, using smoothing at each time step. The value used for ϵ was 0.5. Figure 6.3 shows the corresponding time history for this modified scheme, compared to normal Roe.

There is significant improvement in the oscillations, however we have slightly modified the other properties of the solution. Notice in particular the loss in height at, and after the oscillations; this loss is not recovered later on in time. Increasing ϵ results in the oscillations being reduced in size, however, the deterioration described above increases. As we reduce ϵ the oscillations grow, and the

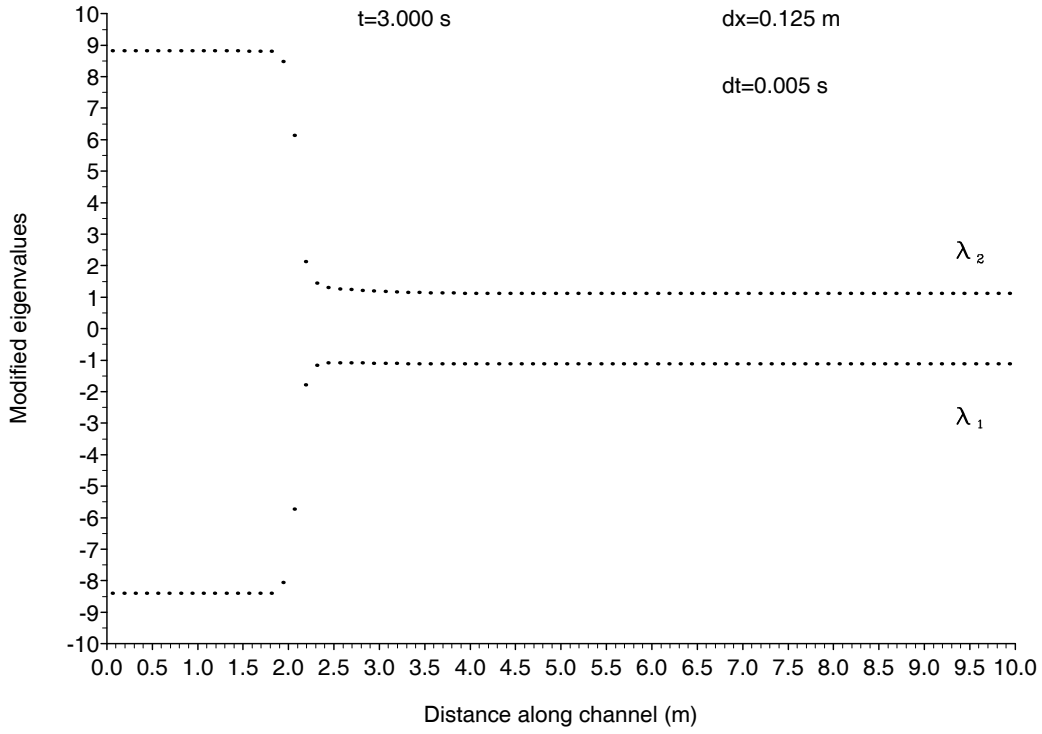

Figure 6.2: Modified eigenvalues from using the modified Roe's scheme ($\epsilon = 0.5$)

solution tends to the unmodified Roe solution. It appears, visually, that an ϵ of about 0.5 gives the best compromise between size of oscillations, and deterioration of solution.

This method is not a very elegant and convincing way of doing things. However, it indicates that the size of oscillations is related to the sharpness of the jump in the wave speeds. Next we shall see a way of doing virtually the same thing, but in a more elegant way.

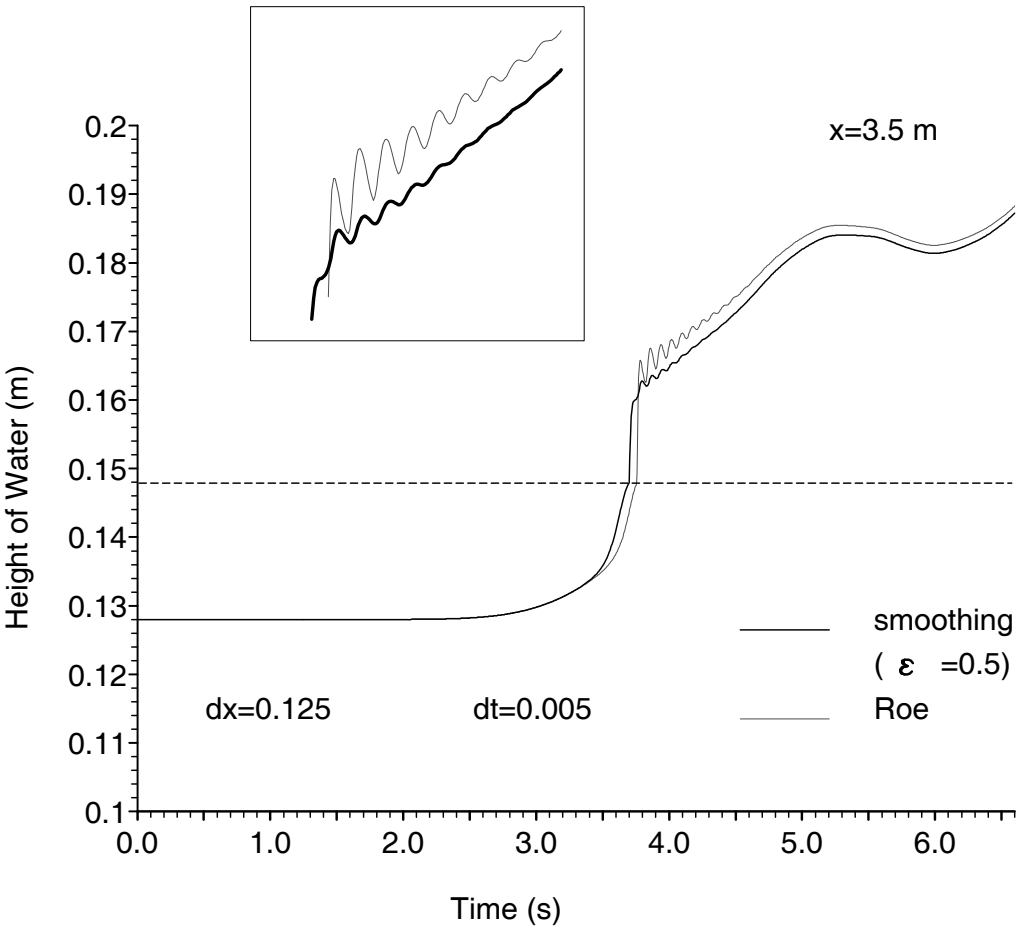

Figure 6.3: Results using modified Roe's scheme ($\epsilon = 0.5$)

6.2 Sloped Roof Technique

The sharp jump in the eigenvalues, in Roe's scheme, is due to the sudden jump in the channel width from w_{ch} to w_{sl}. Another way to make the jump in the eigenvalues less sharp, is to make the channel go from width w_{ch} to width w_{sl} in a continuous manner. The simplest way of doing this is to make the channel width vary linearly from w_{ch} to w_{sl} in a height 2ϵ. See figure 6.4.

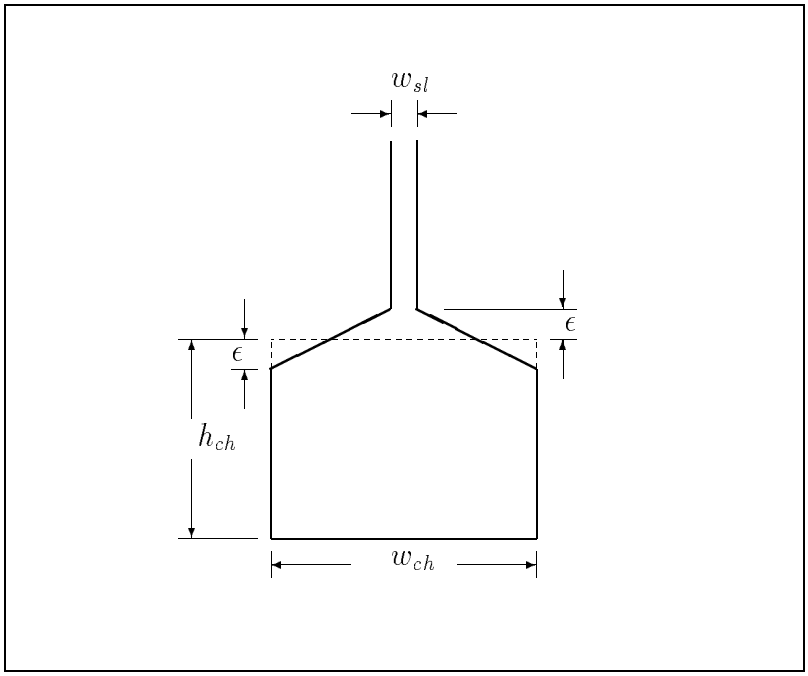

Figure 6.4: Channel with sloped roof.

The channel width is then given as follows,

$$b(h) = \begin{cases} w_{sl} & \text{if } h \geq h_{ch} + \epsilon \\ \dfrac{(w_{sl} - w_{ch})(h - h_{ch})}{2\epsilon} + \dfrac{(w_{ch} + w_{sl})}{2} & \text{if } h_{ch} - \epsilon < h < h_{ch} + \epsilon \\ w_{ch} & \text{if } h \leq h_{ch} - \epsilon \end{cases} \tag{6.1}$$

This is the only way that could be found of continuously varying the width such as to make such things as the integral I_1 and the hydraulic radius easy to calculate.

Since the slot is just a mechanism for simulating pressurized flow, using the

open channel equations, we are not losing much by this alteration as long as ϵ is small. Also when the water is above the linearly varied width region ($h > h_{ch} + \epsilon$), the wetted area for a given height will be the same as if we had not made the alteration. This is because we have not created any new volume in the channel.

Figure 6.5 shows the integral I_1 for the modified channel; I_1 is now differentiable at $A = A_{crit}$. Moreover c (figure 6.6) is now continuous at this point, and its smoothness can be controlled by varying ϵ.

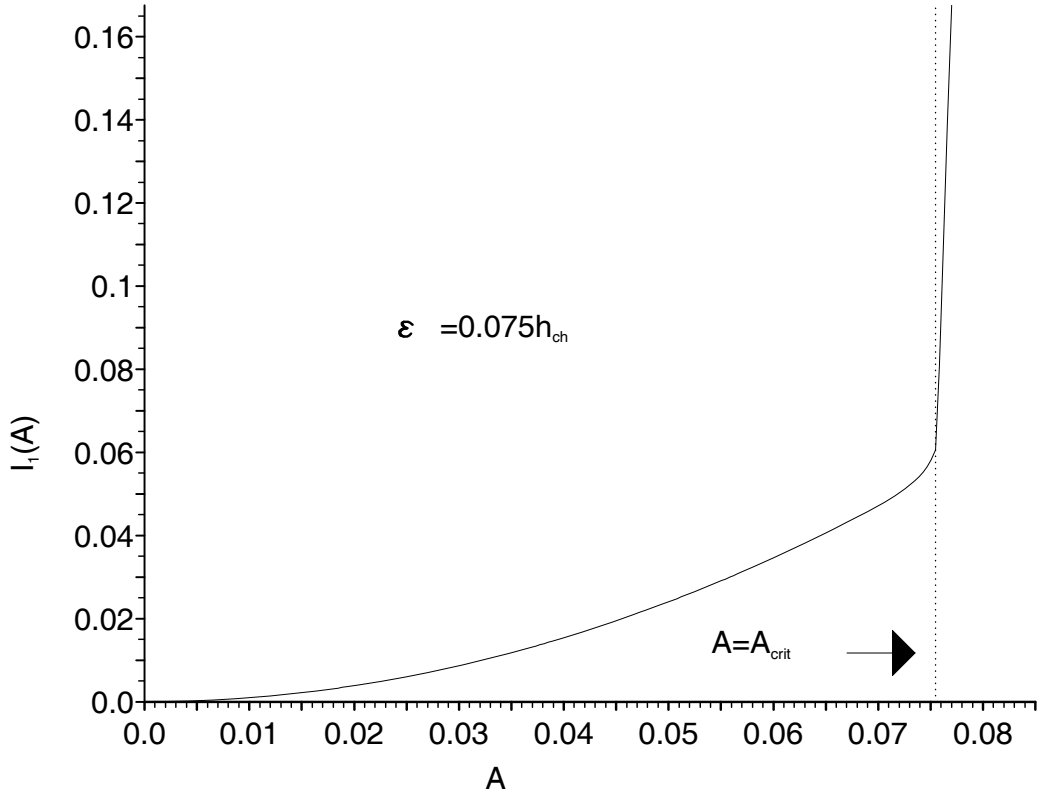

Figure 6.5: $I_1(A)$ for modified channel ($\epsilon = 0.075 h_{ch}$).

6.2.1 Results and Discussion

For this technique we have to make the same compromise as for the method in section 6.1. Figure 6.7 shows the results for $\epsilon = 0.075 h_{ch}$; they are slightly

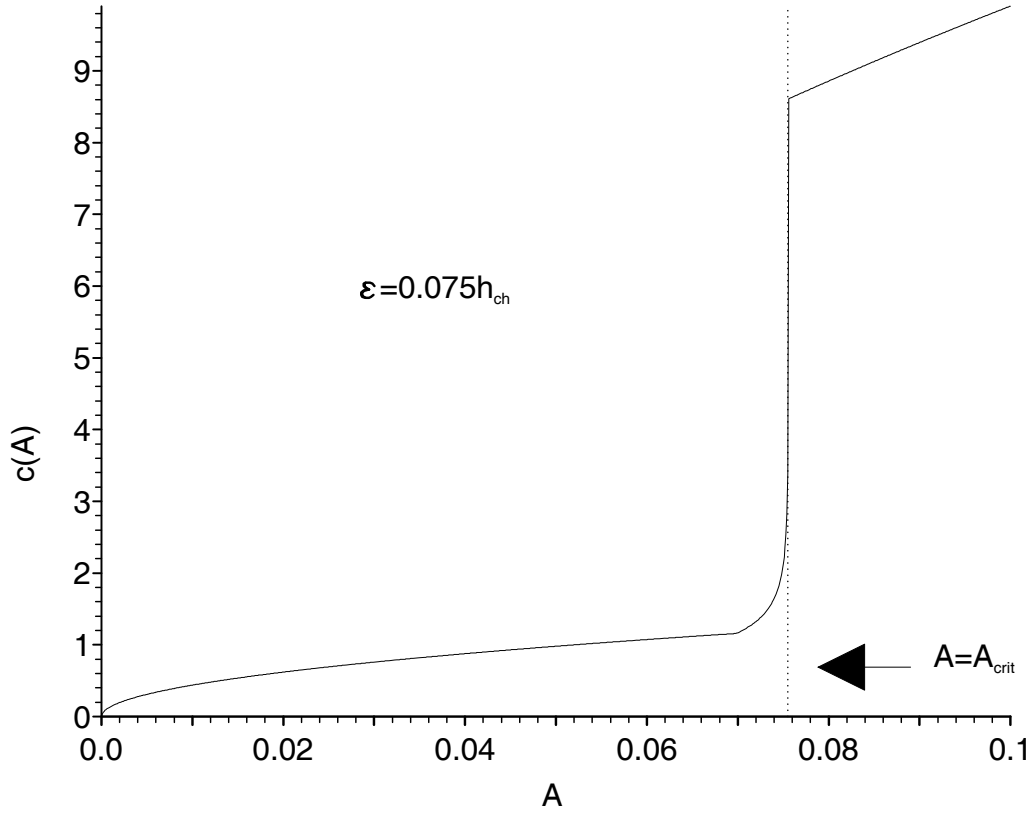

Figure 6.6: $c(A)$ for modified channel ($\epsilon = 0.075 h_{ch}$).

better than when smoothing the eigenvalues, since we do not lose height after the oscillations as in that method. Figure 6.8 shows the results for $\epsilon = 0.11 h_{ch}$; notice the further deterioration of the solution, but the smaller oscillations. An ϵ of about $0.075 h_{ch}$ was found to give, visually, the best results.

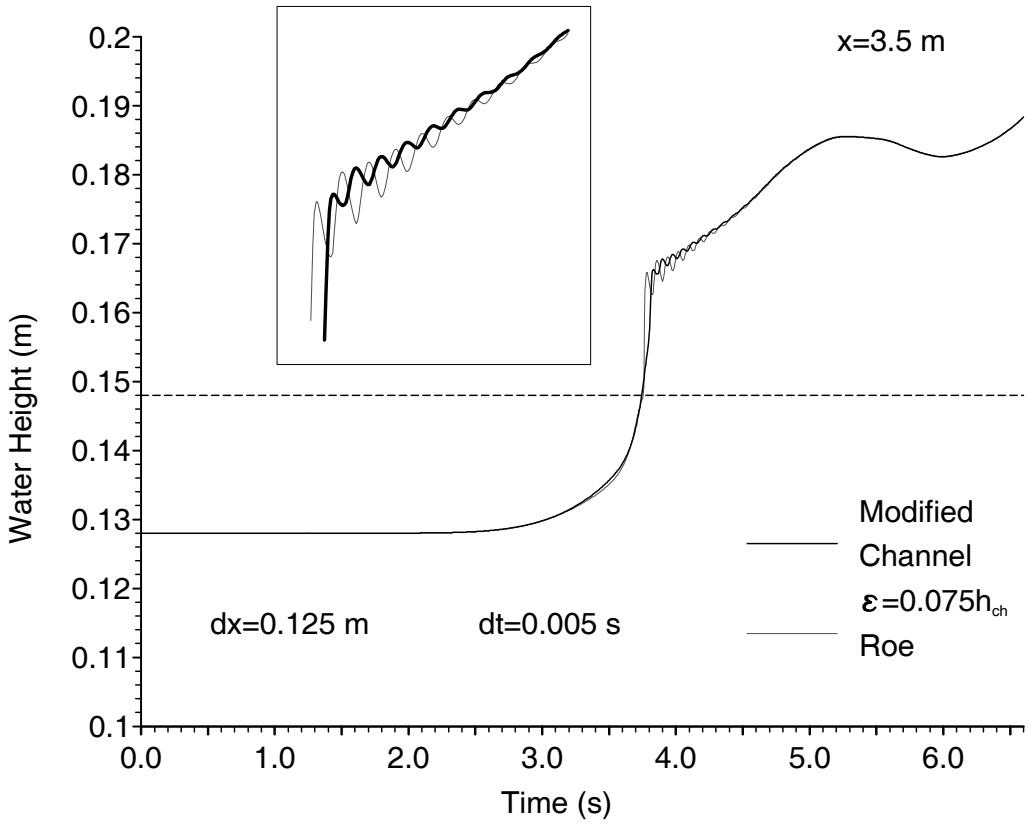

Figure 6.7: Results using modified channel ($\epsilon = 0.075h_{ch}$), against unmodified channel.

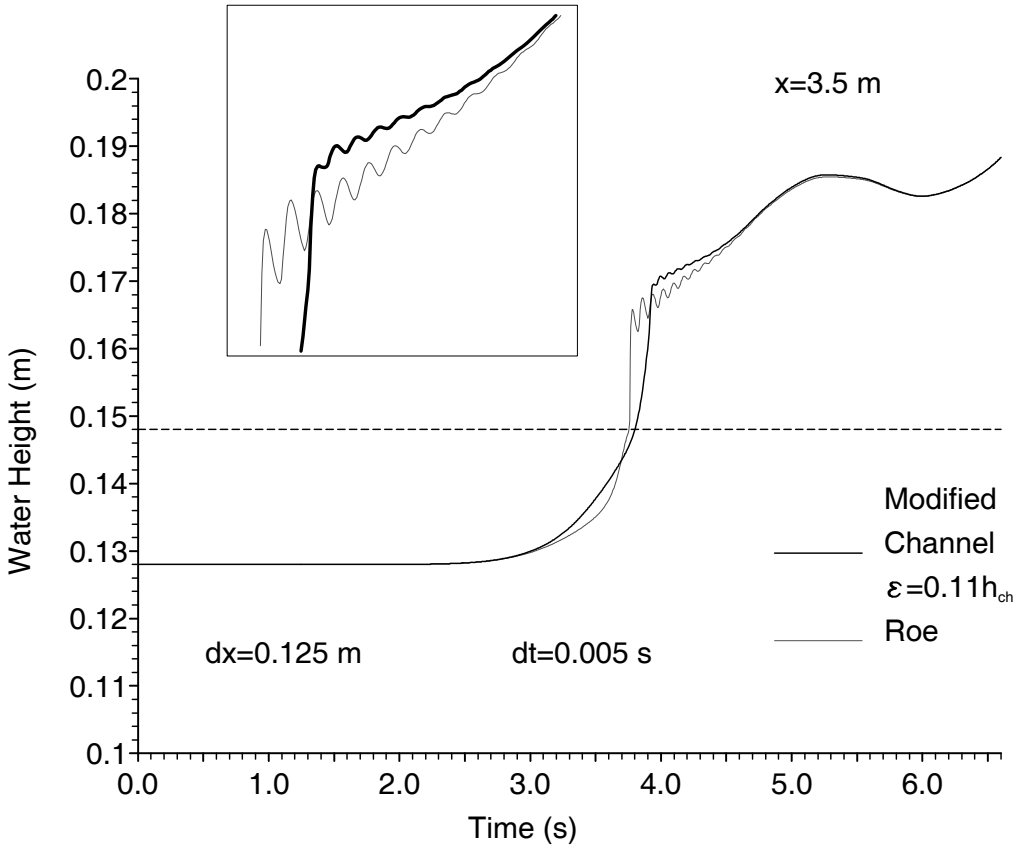

Figure 6.8: Results using modified channel ($\epsilon = 0.11h_{ch}$), against unmodified channel.

Chapter 7

Different Schemes Using Roe Decomposition

Roe's scheme can be written in the following form

$$\frac{\mathbf{W}^{n+1} - \mathbf{W}^n}{\Delta t} = \mathbf{G}(\mathbf{W}^n) \tag{7.1}$$

where

$$\mathbf{W}^n = \begin{bmatrix} \mathbf{w}_0^n \\ \mathbf{w}_1^n \\ \vdots \\ \mathbf{w}_N^n \end{bmatrix}, \mathbf{G}(\mathbf{W}) = \begin{bmatrix} \mathbf{g}_0 \\ \mathbf{g}_1 \\ \vdots \\ \mathbf{g}_N \end{bmatrix}.$$

$\mathbf{g}_j$ is the Roe approximation of

$$\left(-\frac{\partial \mathbf{F}(\mathbf{w})}{\partial x} + \mathbf{D} \right) \Big|_{x = j\Delta x}$$

using the states $\mathbf{W}$. Where we mean the usual Roe approximation to the space derivative of $\mathbf{F}$ and the upwinding approximation to $\mathbf{D}$ (as in section 3.1).

7.1 Implicit Roe's Scheme

One way to make Roe's scheme implicit is in the following way,

$$\frac{\mathbf{W}^{n+1} - \mathbf{W}^n}{\Delta t} = \mathbf{G}(\mathbf{W}^{n+\theta})$$

where

$$\mathbf{W}^{n+\theta} = (1-\theta)\mathbf{W}^n + \theta\mathbf{W}^{n+1}.$$

An iterative method is needed to carry out this scheme, since $\mathbf{W}^{n+1}$ is unknown. We initially set $\mathbf{W}^{n+1} = \mathbf{W}^n$, then use the scheme to calculate a better approximation to $\mathbf{W}^{n+1}$; this value is then used to get a better approximation, and so on. We stop the process when we have got an accurate enough value. Of course we need to implement the boundary conditions as usual, after the iteration has converged.

Implicit schemes are well known to be more stable, than their corresponding explicit schemes. This probably contributes to a good improvement in the oscillations; see figure 7.1 for results for $\theta = 1$. There is a similar improvement as for the smoothing techniques, but in this case there is no deterioration in the solution. The implicit scheme is much more time consuming than the explicit version, and this may make it impractical. The best value for θ was found to be 1.0.

Figure 7.2 shows results from using the implicit scheme, with the modified channel ($\theta = 1, \epsilon = 0.75h_{ch}$). These are probably the best results seen so far; the oscillations are very small, and the rest of the solution compares well with Roe.

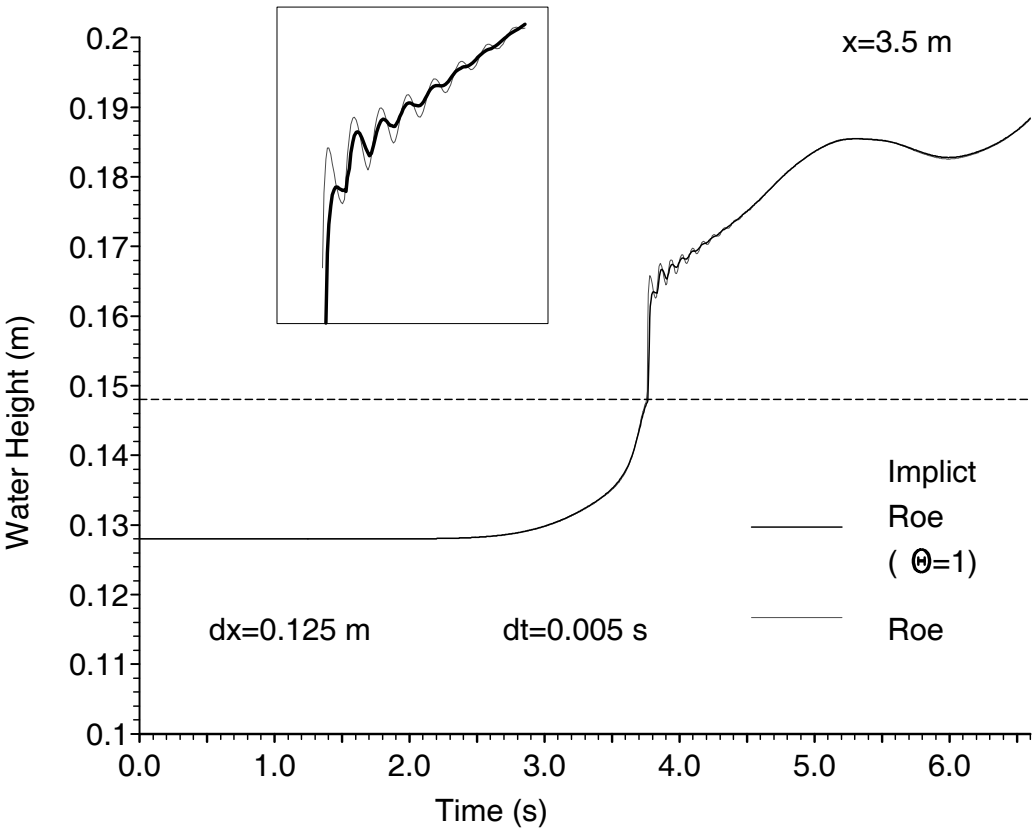

Figure 7.1: Results using implicit Roe's scheme ($\theta = 1$)

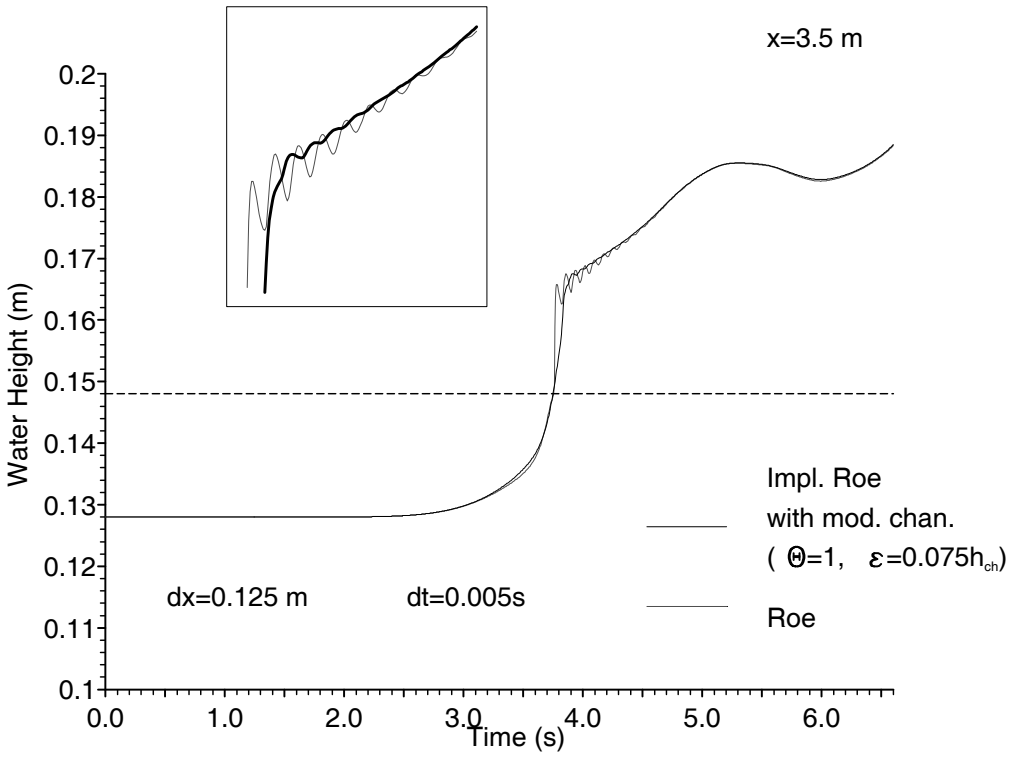

Figure 7.2: Results from implicit Roe with modified channel.($\theta = 1, \epsilon = 0.075 h_{ch}$)

7.2 Alternative Time Stepping

From equation 7.1 it can be seen that Roe's scheme uses Euler time stepping. It would be an idea to try and change to a different time stepping, in order to see what difference this would make. See [10] for more information on different time steppings. First we tried using Runge-Kutta fourth-order as follows,

$$\mathbf{W}^{n+1} = \mathbf{W}^n + \frac{\Delta t}{6}(\mathbf{K}_1 + 2\mathbf{K}_2 + 2\mathbf{K}_3 + \mathbf{K}_4)$$

where

$$\begin{aligned}
\mathbf{K}_1 &= \mathbf{G}(\mathbf{W}^n) \\
\mathbf{K}_2 &= \mathbf{G}(\mathbf{W}^n + \tfrac{\Delta t}{2}\mathbf{K}_1) \\
\mathbf{K}_3 &= \mathbf{G}(\mathbf{W}^n + \tfrac{\Delta t}{2}\mathbf{K}_2) \\
\mathbf{K}_4 &= \mathbf{G}(\mathbf{W}^n + \mathbf{K}_3).
\end{aligned}$$

The Runge-Kutta fourth-order scheme results in a slight improvement in the oscillations, but not as much as the implicit scheme in the previous section. This can be seen from the results in figure 7.3.

Linear Multistep Methods were also tried, including implicit ones; some were unstable and needed the CFL number reducing. None of these gave an improvement better than the implicit scheme described in the previous section.

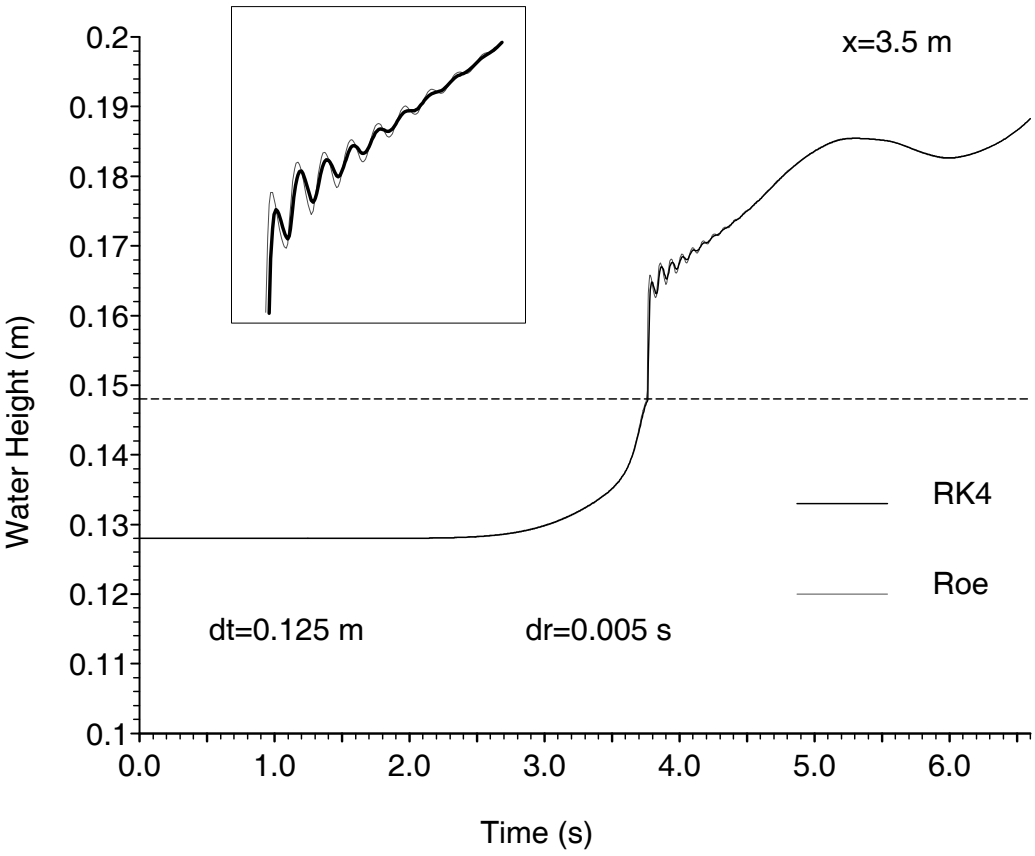

Figure 7.3: Runge-Kutta fourth-order time stepping.

Chapter 8

'Shock' Fitting

8.1 Description

There is now quite a lot of evidence indicating that the problem is due to piecewise constant states, approximating sharply varying functions. In this problem, the front at the pressurized/free surface interface is so sharp that we could treat it like a discontinuity. If we were to ensure that the front was at the interface between two grid cells, then the solution in both the neighbouring cells would be smooth; hence piece-wise constants would then be a valid approximation. In order for us to do this, we will need to work on a non-uniform grid and allow the grid to alter in time. We will also need to be able to find and keep track of the position of the front. The following is a simple way of achieving the above, by modifying Roe's scheme.

Step 1: Finding the Front.

Until the front develops, and is found, we proceed as before with the ordinary Roe's scheme. The following criterion is used to identify the front, and calculate

its position (see [6]). The front is in cell k if all of the following hold.

$$r_k > 0, \qquad |r_{k-1}| \ll 1, \qquad |r_{k+1}| \gg 1$$

with

$$A^n_{k-1} \geq A_{crit} \quad and \quad A^n_{k+1} \leq A_{crit}.$$

r_j is given by

$$r_j = \frac{h^n_j - h^n_{j-1}}{h^n_{j+1} - h^n_j}$$

where h^n_j is the water height corresponding to area A^n_j.

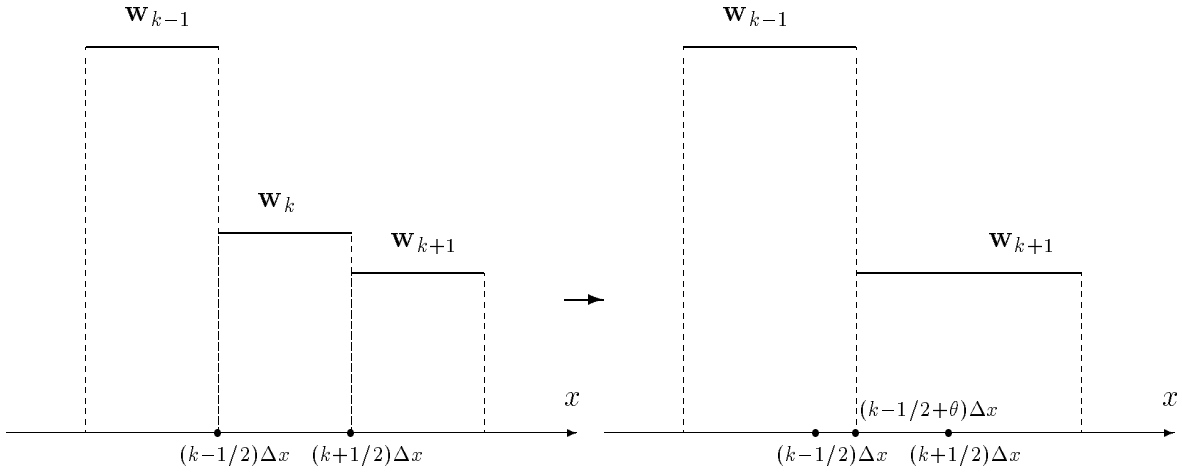

Figure 8.1: Replacement of three states by one discontinuity .

We find the position of the front by using conservation of mass to replace the three states near cell k (see figure 8.1), by a single discontinuity. If the discontinuity is at $x_s = (k - 1/2 + \theta)\Delta x$ then θ is given by

$$\theta = \frac{A^n_{k+1} - A^n_k}{A^n_{k+1} - A^n_{k-1}}.$$

Note that Q will only be conserved by this process if the front in Q is at the same position as the front in A.

Step 2: Modification of Grid.

We next need to place the front at the interface, between two cells. This is done by eliminating cell k and extending the size of its two neighbours, in such a way that we end up with the second part of figure 8.1. We now get a new set of states, of non-uniform size

$$\mathbf{w}_j^\star = \begin{cases} \mathbf{w}_j^n & \text{if} \quad j \leq k-1 \\ \mathbf{w}_{j+1}^n & \text{if} \quad j > k-1 \end{cases} .$$

State j has width $f_j \Delta x$, where f_j is given by the following

$$f_j = \begin{cases} 1+\theta & \text{if} \quad j = k-1 \\ 2-\theta & \text{if} \quad j = k \\ 1 & \text{otherwise.} \end{cases} .$$

Step 3: Application of Roe's scheme to the new set of states.

We now apply Roe's scheme to these new set of states, but because the cells are not all the same size we need a few changes. For each Riemann problem we calculate the eigenvalues and wave strengths exactly as before. The change comes in the updating; the modified procedure is as follows. For the j^{th} Riemann problem we calculate and keep the following

$$\left.\begin{aligned} \tilde{\lambda}_{i,j+1/2} &= \tilde{\lambda}_i \\ \mathbf{\Phi}_{i,j+1/2} &= \begin{cases} \left(-\dfrac{\Delta t}{f_{j+1}\Delta x}\tilde{\lambda}_i\tilde{\alpha}_i + \Delta t\tilde{\beta}_i\right)\tilde{\mathbf{e}}_i & \text{if} \quad \tilde{\lambda}_i > 0 \\ \left(-\dfrac{\Delta t}{f_j\Delta x}\tilde{\lambda}_i\tilde{\alpha}_i + \Delta t\tilde{\beta}_i\right)\tilde{\mathbf{e}}_i & \text{if} \quad \tilde{\lambda}_i \leq 0 \end{cases} \end{aligned}\right\} i = 1, 2$$

This is carried out for $j = 0, 1, \ldots, N-2$.

We now use the following procedure to update the solution to the next time level,

For $j = 0, 1, \ldots, N-2$

$$\left.\begin{array}{l} \text{if } \tilde{\lambda}_{i,j+1/2} > 0 \text{ then increment } \mathbf{w}^\star_{j+1} \text{ by } \mathbf{\Phi}_{i,j+1/2}, \\ \text{else increment } \mathbf{w}^\star_{j} \text{ by } \mathbf{\Phi}_{i,j+1/2}. \end{array}\right\} i = 1, 2$$

Step 4: Finding the new position of front.

We now have values for the states at the new time level and we use these to find the new position of the front.

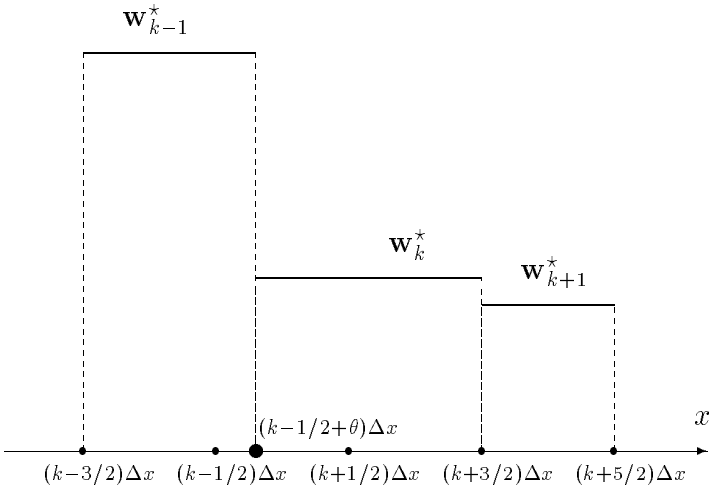

Figure 8.2: Finding the new position of front using three states.

We now use the three states, shown in figure 8.2, to get the new position of the front. We do this in the same way as step 1. The new value for θ given by

$$\theta' = (1-\theta)\left(\frac{A^\star_{j+1} - A^\star_j}{A^\star_{j+1} - A^\star_{j-1}}\right)$$

Figure 8.3 shows the resulting discontinuity.

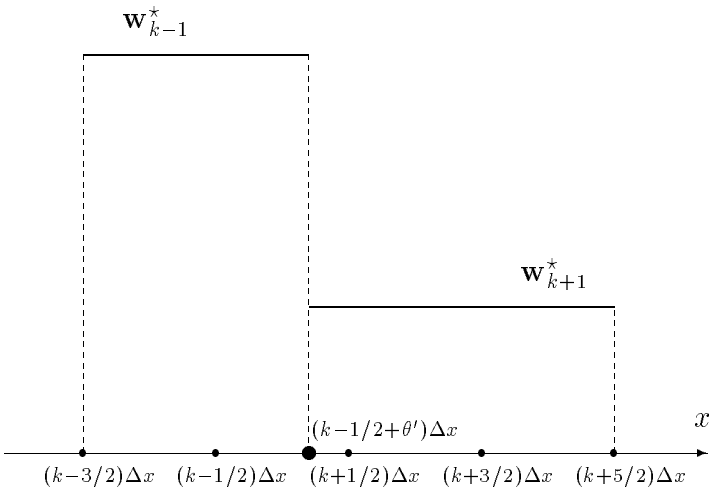

Figure 8.3: New position of discontinuity.

Step 5: Recovering the original uniform states.

We now wish to get values for the original uniform grid that we started with. There is no unique way of doing this. After trying several ways, it was found that the following worked best,

$$\mathbf{w}_j^{n+1} = \begin{cases} \mathbf{w}_j^{\star} & \text{if} \quad j \leq k-1 \\ \mathbf{z}_1 & \text{if} \quad j = k \\ \mathbf{z}_2 & \text{if} \quad j = k+1 \\ \mathbf{w}_{j-1}^{\star} & \text{if} \quad j \geq k+2 \end{cases}$$

where $\mathbf{z}_1, \mathbf{z}_2$ will be defined below.

In order to fix up $\mathbf{z}_1$ and $\mathbf{z}_2$ we need two pieces of information. The two things chosen were conservation and the position of the front. Depending on the value of θ' we needed to do the following.

If $\theta' \leq 1$ then the front has not moved cells. From conservation we get

$$\mathbf{z}_1 + \mathbf{z}_2 = \theta' \mathbf{w}^\star_{k-1} + (1 - \theta')\mathbf{w}^\star_{k+1}.$$

The new position of the front gives

$$\theta' \mathbf{w}^\star_{k-1} + (1 - \theta')\mathbf{z}_2 = \mathbf{z}_1.$$

We solve these two equations for $\mathbf{z}_1$ and $\mathbf{z}_2$.

If $\theta' > 1$ then the front has moved one cell to the right. From conservation we get

$$\mathbf{z}_1 + \mathbf{z}_2 = \theta' \mathbf{w}^\star_{k-1} + (1 - \theta')\mathbf{w}^\star_{k+1}.$$

The new position of the front gives

$$(\theta' - 1)\mathbf{z}_1 + (2 - \theta')\mathbf{w}^\star_{k+1} = \mathbf{z}_2.$$

We solve these two equations for $\mathbf{z}_1$ and $\mathbf{z}_2$.

We are now in the position to do another time step. We now know the new position of the front, so we need never repeat step 1 again; we can just start with step 2.

8.2 Results and Discussion

Figure 8.4 shows result for this 'shock' fitting method. The results are extremely good; there is not a sign of an oscillation. The solution behaves slightly peculiarly just before the height starts to rise sharply, and again after it has finished rising (see magnified regions in figure). These peculiarities do not appear to be too

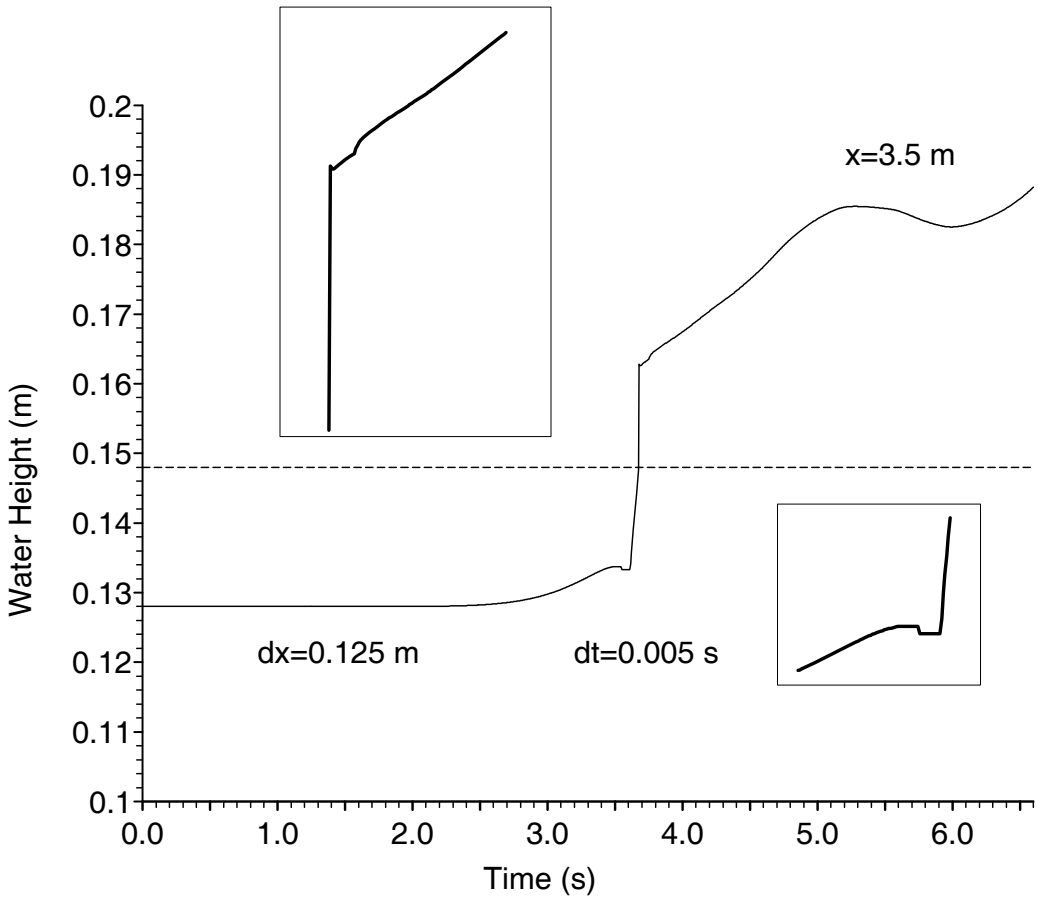

Figure 8.4: Results with 'shock' fitting.

serious, and are much better than having oscillations. Figure 8.5 is a comparison of these results against Roe. From this it seems as if we have a slight deterioration in the solution. If we run Roe on an eight times finer grid with an eight times smaller time step, it can be seen, from figure 8.6 that the 'shock' fitting method compares very well with the results.

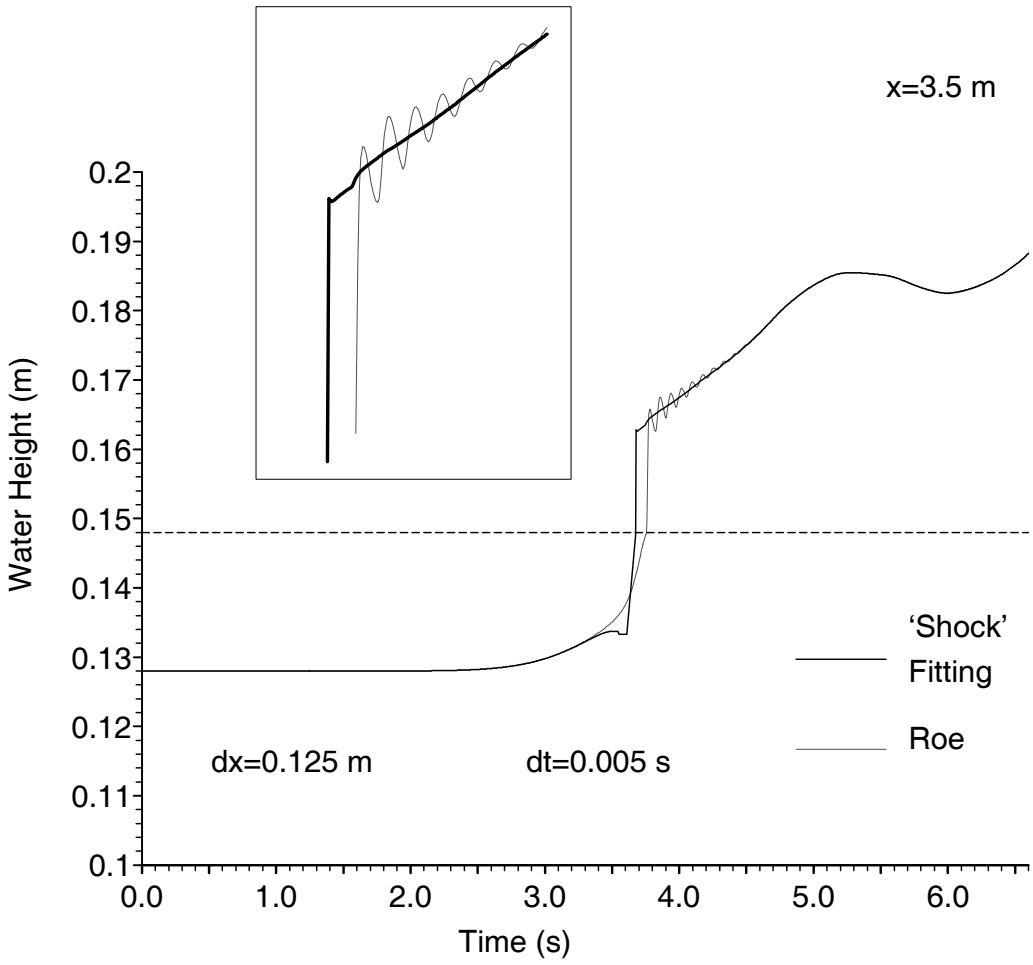

Figure 8.5: Results with 'shock' fitting compared with Roe.

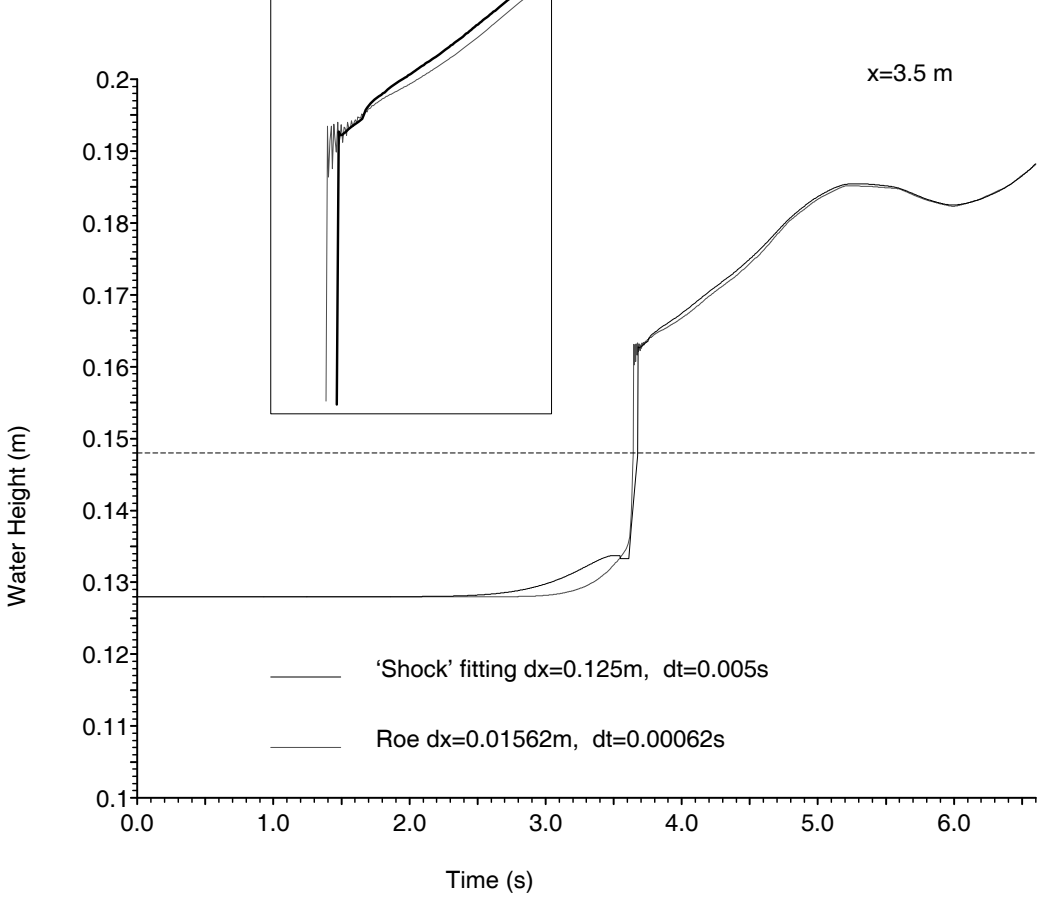

Figure 8.6: Results with 'shock' fitting compared with Roe on a very fine grid.

This 'shock' fitting approach seems very promising, and has plenty of scope for improvement, especially in step 5. It should not be too hard to make a more refined version. The scheme is to all intents and purposes conservative. The only slight exception, is when we find the front for the first time. At this time we assume the fronts in both Q and A are at the same position. This assumption does not appear to be too unreasonable.

An alternative process to that described in this chapter is, instead of eliminating a cell, to subdivide the cell containing the front. The major drawback of this alternative way is that we will sometimes get very small cells. This results in us needing a very small time step, in order to satisfy the CFL condition. By extending the cells we are sure that the minimum cell size is always Δx.

Chapter 9

Conclusions

Throughout this work, we have been unable to pinpoint, exactly, the cause of the oscillations; however it is felt that we have gone some way to understanding the cause.

In chapter 5 it was concluded that the approximate nature of the Riemann solvers was not a significant factor in causing the oscillations. The approximation of piecewise constant states seemed to play a much bigger part. The first significant improvement in the oscillations was found with the smoothing techniques, however these are seriously limited by the deterioration of the solution. The implicit scheme from section 7.1 did not cause such deterioration, but was very slow, and has limited scope for improvement. The most promising method found was the 'shock' fitting approach in chapter 8. For our problem this approach gave very good results, with the total elimination of the oscillations, although we have found that for a more severe problem where the pressurized flow has a more realistic wave celerity, the oscillations do return. Given time, there is much scope for improving and refining this method, and it seems likely that this is the most

fruitful direction. Another approach that might be considered is increasing the order of approximation, eg. using piecewise linears.

Bibliography

[1] **Baines,M.J. & Maffio,A. & Di Flippo,A.**, Unsteady 1-D Flows with Steep Waves in Plant Channels: The Use of Roe's Upwind TVD Difference Scheme. Advances in Water Resources, v. 15, 1992, pp. 89-94.

[2] **Cunge,J.A. & Holly,F.M. & Verwey,.A.**, Practical Aspects of Computational River Hydraulics. Pitman Advanced Publishing Program, 1980.

[3] **Emmerson,S.**, Modelling of Transient Dynamics of Gas Flow in Pipes. Ph.D. Thesis, University of Reading, 1991.

[4] **Godunov,S.K.**, A Finite Difference Method for the Numerical Computation of Discontinuous Solutions of the Equations of Fluid Dynamics. Mat.Sb. v. 47, 1959, pp. 271-306.

[5] **Hirsch,C.**, Numerical Computation of Internal and External Flows. Volume 2: Computational Methods for Inviscid and Viscous Flows. John Wiley & Sons, 1990.

[6] **Morton,K.W. & Sweby,P.K.**, A Comparison of Flux Limited Difference Methods and Characteristic Galerkin Methods for Shock Modelling. Journal of Computational Physics. v.73, 1987, pp. 203-230.

[7] **Osher,S. & Solomon,F.**, Upwind Difference Schemes for Hyperbolic Systems of Conservation Laws. Mathematics of Computation. v. 38, 1982, pp. 339-374.

[8] **Priestly,A.**, Roe Type Schemes for the 2-D Shallow Water Equations. Reading University Numerical Analysis Report 8/87.

[9] **Roe,P.L.**, Approximate Riemann Solvers, Parameter Vectors, and Difference Schemes. Journal of Computational Physics. v.43, 1981, pp. 357-372.

[10] **Shu,C-W.**, Total-Variation-Diminishing Time Discretizations. SIAM J. Sci. Stat. Comput. v. 9, 1988, pp. 1073-1084

[11] **Smoller,J.**, Shock Waves and Reaction-Diffusion Equations. Springer-Verlag, 1983.

[12] **Stoker,J.J.**, Water Waves: The Mathematical Theory with Applications. Interscience publishers, Inc., New York, 1957.

[13] **Vila,J.P.**, Simplified Godunov Schemes For 2x2 Systems of Conservation Laws. J. Numer. Anal. v. 23, 1986, pp. 1173-1191.

[14] **Wiggert,D.C.**, Transient Flow In Free-Surface, Pressurized Systems. Journal of the Hydraulics Division, Proceedings of the American Society of Civil Engineers, v.98 No. HY1, 1972, pp. 11-27.